

In Vitro and In Silico Investigation of Water-Soluble Fullereneol $C_{60}(OH)_{24}$: Bioactivity and Biocompatibility

Vladimir V. Sharoyko,* Nailia R. Iamalova, Sergei V. Ageev, Anatolii A. Meshcheriakov, Gleb O. Iurev, Andrey V. Petrov, Dmitry A. Nerukh, Vladimir S. Farafonov, Lubov V. Vasina, Anastasia V. Penkova, and Konstantin N. Semenov*



Cite This: *J. Phys. Chem. B* 2021, 125, 9197–9212



Read Online

ACCESS |



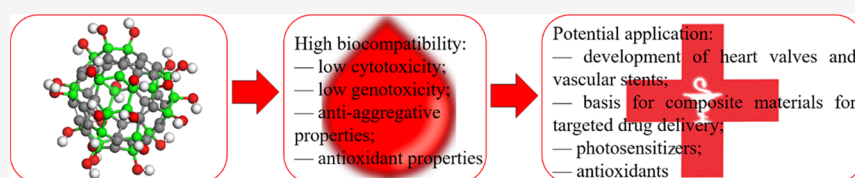
Metrics & More



Article Recommendations



Supporting Information



ABSTRACT: Light fullerenes, C_{60} and C_{70} , have significant potential in biomedical applications due to their ability to absorb reactive oxygen species, inhibit the development of tumors, inactivate viruses and bacteria, and as the basis for developing systems for targeted drug delivery. However, the hydrophobicity of individual fullerenes complicates their practical use; therefore, creating water-soluble derivatives of fullerenes is increasingly important. Currently, the most studied soluble adducts of fullerenes are polyhydroxy fullerenes or fullereneols. Unfortunately, investigations of fullereneol biocompatibility are fragmental. They often lack reproducibility both in the synthesis of the compounds and their biological action. We here investigate the biocompatibility of a well-defined fullereneol $C_{60}(OH)_{24}$ obtained using methods that minimize the content of impurities and quantitatively characterize the product's composition. We carry out comprehensive biochemical and biophysical investigations of $C_{60}(OH)_{24}$ that include photodynamic properties, cyto- and genotoxicity, hemocompatibility (spontaneous and photo-induced hemolysis, platelet aggregation), and the thermodynamic characteristics of $C_{60}(OH)_{24}$ binding to human serum albumin and DNA. The performed studies show good biocompatibility of fullereneol $C_{60}(OH)_{24}$, which makes it a promising object for potential use in biomedicine.

1. INTRODUCTION

Polyhydroxylated fullerenes (fullereneols) are currently the most studied class of water-soluble derivatives of fullerenes.^{1–6} Fullereneols exhibit high antioxidant activity, radioprotective, antimutagenic, antitumor, and antimetastatic properties.^{7–16} Due to their low toxicity^{1,17–21} and chemical structure convenient for immobilization of various biologically active molecules, fullereneols are promising drug carriers.^{17,22–25}

Saitoh et al.¹⁰ studied the possibility of using the fullereneol $C_{60}(OH)_{24}$ as a radioprotector and found that it prevents the radiation-induced decrease in the leukocyte level and exhibits radioprotective properties most effectively in the spleen, small intestine, and lungs of rats.

The antioxidant properties of fullereneols were first described under the conditions of inducing reactive oxygen species (ROS) production caused by the reversible damage to the hippocampus for *in vitro*,²⁶ as well as *in vivo* models of dogs with intestinal ischemia-reperfusion and small bowel transplantation.²⁷ It was later shown that $C_{60}(OH)_{24}$ can trap the radicals of nitrogen monoxide when sodium nitroprusside (NO-radical donor) is added to the solution.⁹ In recent studies, a correlation was found between the antioxidant properties of $C_{60}(OH)_{24}$ and the activity of nuclear factor erythroid 2-related factor 2 (NRF2), which regulates the expression of antioxidant enzymes.²⁸

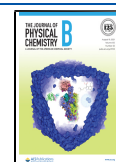
Fullerenes can be used as photosensitizers. The ability of fullerene C_{60} and its water-soluble derivative $C_{60}(OH)_{18}$ to damage cell membranes after photoactivation was studied with rat liver microsomes. It was shown that fullerene and fullereneol can generate ROS as a result of photoexcitation and cause lipid peroxidation and oxidation of cell membrane proteins.²⁹

Another application of fullereneols, associated with the delivery of anticancer drugs, is proposed in ref 24. The fullereneol–doxorubicin conjugate ($C_{60}(OH)_{18–24}$ –Dox) inhibited *in vitro* proliferation of tumor cell lines (mouse melanoma B16–F10, mouse lung carcinoma LLC1, and metastatic human breast carcinoma MDA-MB231) by blocking the G2-M cell cycle phase leading to apoptosis. *In vivo* experiments in mice showed high antitumor efficacy of the fullereneol–Dox conjugate without the systemic toxicity of free Dox.

Received: April 13, 2021

Revised: July 21, 2021

Published: August 10, 2021



The protective function of $C_{60}(OH)_{24}$ against Dox-induced hepatotoxicity in experiments was studied *in vivo* (using Sprague Dawley rats) and *in vitro* (using human HepG2 hepatocellular carcinoma and Caco-2 colorectal adenocarcinoma).³⁰ The authors found that it can serve as a potential hepatoprotector under the conditions of Dox-induced hepatotoxicity.

Xu et al.³¹ found that the fullerenols $C_{60}(OH)_x$ ($x = 22, 24$) can reduce the toxic effects of some dangerous toxicants. For example, a model based on hepato- and nephrotoxicity, caused by the action of carbon tetrachloride (CCl_4), was used to study the protective mechanisms of fullereneol in Sprague Dawley rats. It was found that the liver and kidney were protected against CCl_4 -induced oxidative stress by activating the antioxidant defense systems.

Fullerenols have a positive effect on the development, yield, and quality of various crops. Panova et al.³² and Bityutskii et al.³³ developed nanocompositions containing fullerenols $C_{60}(OH)_{n1}O_{n2}$ and various trace elements that led to increased crop yields, improved crop quality, reduced ripening period of fruits and vegetables, reduced degree of disease damage to plants, increased plant resistance to adverse environmental conditions (winter hardness, drought tolerance), increased seed germination, and reduced level of nitrates in plants.

To summarize, fullerenols are the most studied class of water-soluble fullerene derivatives. The study of this class of compounds began more than 20 years ago, and to date, a fairly large array of information has been accumulated on the production, the physicochemical and biological properties, as well as on the use of fullerenols. However, the literature on the biological properties and biocompatibility of water-soluble fullerene derivatives shows systematic limitations in their studies. They include the following:

1. Most studies lack comprehensive data on the quantitative identification of fullerenols.
2. The proposed synthesis methods often do not provide compounds with a reproducible composition of the final product.
3. It is known that in addition to hydroxyl groups, fullerenols may contain other functional groups (oxo, epoxy, carboxy, etc.); it should also be noted that most of the methods for the synthesis of fullerenols are carried out in alkaline medium,^{3,34–36} thus, fullerenols can exist in the form of salts.
4. The studies of the biological properties and biocompatibility of fullerenols are fragmentary. The reason is the low reproducibility of the composition of the studied adducts (see the points above).

All of these make it very difficult to investigate the biomolecular mechanisms of fullerenols' action.

We address the above deficiencies in the present work and report on the studies of the biocompatibility of the well-defined fullereneol $C_{60}(OH)_{24}$. This adduct was obtained under mild conditions by alkaline hydrolysis of a bromo derivative $C_{60}Br_{24}$. The use of this technique made it possible to obtain a reproducible composition of the final product with a minimum content of impurity groups.^{9,37–39} Thus, in this work, for the first time, a comprehensive study of the biocompatibility of the aqueous $C_{60}(OH)_{24}$ solutions was carried out.

The study of biocompatibility is a key point for preclinical studies and a starting point for further applications of this adduct in nanobiomedicine. No doubt, the uniqueness of the electronic structure of fullerenols, its compatibility with water and aqueous

solutions, the presence of an internal volume, and the possibility of immobilization of biologically active molecules make this class of compounds extremely promising for biology and medicine. Here, we investigate the thermodynamic characteristics of the binding of fullereneol to human serum albumin (HSA) and DNA, genotoxicity, platelet aggregation, erythrocyte hemolysis (spontaneous and photo-induced), and photodynamic properties. As the first step in the investigation of biomolecular mechanisms behind the fullerenols' activity, the molecular dynamics (MD) simulations were carried out to study the process of $C_{60}(OH)_{24}$ self-association in water, as well as the interaction of $C_{60}(OH)_{24}$ with HSA.

2. EXPERIMENTAL SECTION

2.1. Materials. The manufacturers and the purity of the reagents that were used are presented in Table 1. The

Table 1. Provenance and Mass Fraction Purity of the Reagents

| no. | sample | manufacturer | main substance content |
|-----|--|---------------------------|------------------------|
| 1 | $C_{60}(OH)_{24}$ | Ltd ZAO "ILIP", Russia | ≥ 0.998 |
| 2 | HSA | Biolog, Russia | ≥ 0.950 |
| 3 | PBS | Biolog, Russia | |
| 4 | radachlorin | Rada-Pharma, Russia | |
| 5 | dimethyl sulfoxide | Sigma-Aldrich | ≥ 0.997 |
| 6 | sodium azide | Sigma-Aldrich | ≥ 0.995 |
| 7 | ADP | Sigma-Aldrich | ≥ 0.950 |
| 8 | sodium citrate | Sigma-Aldrich | ≥ 0.999 |
| 9 | propidium iodide | Sigma-Aldrich | ≥ 0.940 |
| 10 | hydrogen peroxide | Biolog, Russia | ≥ 0.333 |
| 11 | digitonin | Sigma-Aldrich | ≥ 0.920 |
| 12 | ibuprofen | Sigma-Aldrich | ≥ 0.980 |
| 13 | warfarin | Sigma-Aldrich | ≥ 0.970 |
| 14 | DNA from salmon sperm with an average mass of 350 kDa (by gel electrophoresis) | Technomed service, Russia | ≥ 0.980 |

identification of the obtained $C_{60}(OH)_{24}$ using various physicochemical methods (NMR, IR, UV/Vis spectroscopy, mass spectrometry, elemental analysis) was previously described in refs 40, 41.

2.2. Particle Size Distribution in Aqueous Solutions and ζ -Potentials of $C_{60}(OH)_{24}$. The size distribution of $C_{60}(OH)_{24}$ particles in aqueous solutions in the concentration range $C = 10\text{--}100 \mu\text{M}$ was measured using the Malvern Zetasizer 3000 instrument at 293.15 K temperature; the values of polydispersity indices were 0.24–0.47.

Table 2 shows the results for the particle distribution by size and ζ -potentials. The data shows that in the concentration range $C = 10\text{--}100 \mu\text{M}$, the hydrodynamic diameter of the particles in solution increases from 10 to 40 nm. This is most probably due to the self-association of $C_{60}(OH)_{24}$ molecules via hydrogen bonds and hydrophobic interactions. The concentration dependence of ζ -potentials shows that in this concentration range, the solutions of $C_{60}(OH)_{24}$ are electrokinetically stable.

2.3. Biocompatibility of Fullereneol $C_{60}(OH)_{24}$. **2.3.1. Erythrocyte Hemolysis.** Erythrocyte hemolysis was studied by measuring the optical density of supernatants at the wavelength

Table 2. Size Distribution of $C_{60}(\text{OH})_{24}$ Associates in Aqueous Solutions at 293.15 K^a

| C (μM) | δ_i (nm) | $N_{0 \rightarrow i}$ | ζ (mV) |
|---------------------|-----------------|-------------------------|--------------|
| 0 | 2 ⁴¹ | | |
| 10 | 10 | $\approx 6 \times 10^1$ | -30 |
| 50 | 20 | $\approx 5 \times 10^2$ | -30 |
| 75 | 40 | $\approx 4 \times 10^3$ | -30 |
| 100 | 40 | $\approx 4 \times 10^3$ | -30 |

^a δ_i is the average diameters of i -th order molecules in the solution; $N_{0 \rightarrow i}$ is the average number of $C_{60}(\text{OH})_{24}$ monomeric molecules in clusters of the first order. Calculation of the content of the monomeric molecules in first-order associates was performed using the equation

$N_{0 \rightarrow i} = \left(\frac{\delta_i}{\delta_0}\right)^3 \cdot (K_{\text{pack}})^i$, where δ_0 is the diameter of the $C_{60}(\text{OH})_{24}$ molecule, K_{pack} is the packing coefficient corresponding to the packing of "small spheres" into the "big sphere" (in our case, the value of $K_{\text{pack}} = 0.52$ was chosen);⁶⁸ ζ is the zeta potential of the associates.^{40,42}

of $\lambda = 540$ nm using the SF-2000 spectrophotometer (OKB SPECTR, Russia), as previously described in ref 42.

A total of 1.5 mL of the test mixture was prepared from 750 μL of the $C_{60}(\text{OH})_{24}$ solution with $C = 20$ – 200 μM and 750 μL of the suspension of erythrocytes in physiological saline. After the mixture was prepared, the samples were incubated at 37.0 ± 0.2 °C for 1 and 3 h and centrifuged for 10 min at 6000 rpm. Erythrocyte suspensions with the addition of equivalent volumes of distilled water and physiological saline, respectively, were used as positive and negative controls. The hematocrit values were in the reference interval of healthy donors (0.40–0.46). The concentration dependence of the relative change in hemolysis was calculated using the following equation

$$\text{haemolysis \%} = \frac{A_s - A_0}{A_{100}} \times 100 \% \quad (1)$$

where A_s is the optical density of the sample, A_0 is the optical density of the control, and A_{100} is the optical density of water with the suspension of erythrocytes (100% hemolysis).

2.3.2. Photo-Induced Hemolysis. Erythrocytes were obtained from citrate blood by centrifugation at 1500 rpm for 10 min, followed by three washing cycles with physiological saline. Then, the cells were stabilized for 24 h at 4 °C in Alsever's reagent (2.05% dextrose, 0.8% sodium citrate, 0.055% citric acid, and 0.42% sodium chloride). Before the experiment, the erythrocytes were washed three times in Alsever's reagent with saline. Washing removed plasma residues, leukocytes, platelets, and electrolytes. Further experiments were carried out with the stabilized suspension of erythrocytes. Then, the standard suspension of the erythrocytes with an optical density equal to 0.560 ± 0.020 at 800 nm was prepared after eight-fold dilution with phosphate buffer (pH 7.4).

The antioxidant properties of $C_{60}(\text{OH})_{24}$ were evaluated using a device for the study of photo-induced hemolysis by the method published previously.⁴³ The measurements were performed using the SF-2000 spectrophotometer (Russia) in a cuvette with an optical path length of 5 mm. According to this technique, in a shielded cuvette with an optical path length of 5 mm, the incubation mixture was prepared. The mixture contained 100 μL of the standard suspension of erythrocytes, 600 μL of the phosphate buffer solution (pH 7.4), 80 μL of the solution with various concentrations of $C_{60}(\text{OH})_{24}$ ($C = 10$ – 100 μM), and 20 μL of the photosensitizer Radachlorin (0.35% solution for intravenous administration, the main substance was

(7S,8S)-13-vinyl-5-(carboxymethyl)-7-(2-carboxyethyl)-2,8,12,17-tetramethyl-18-ethyl-7H,8H-porphyrin-3-carboxylic acid). The final concentration of Radachlorin in the sample was 62.5 $\mu\text{g}\cdot\text{mL}^{-1}$. As a control, an incubation mixture containing saline instead of fullereneol was used. Then, 800 μL of the resulting incubation mixture was thermostated in the cuvette compartment of the spectrophotometer for 3 min at 37 °C with constant stirring, and it was irradiated with the red Laserland LED-2000 laser (Besram Technology Inc., China; 659 nm, power 55 mW, irradiation dose 3.5 $\text{J}\cdot\text{cm}^{-2}$). After the completion of irradiation, the decrease in the optical density of the solution at 800 nm was recorded at five-second intervals until complete hemolysis.⁴⁴

Using the recorded hemolytic curve, which had a smooth S-shaped character, TC_{50} was determined, the time from the completion of irradiation to lysis of 50% of erythrocytes in the incubation mixture.⁴³ By changing the value of TC_{50} , the speed of the hemolytic process was estimated.

2.3.3. Effect of $C_{60}(\text{OH})_{24}$ on the Hemostasis Parameters. Clotting tests include methods for measuring activated partial thromboplastin time (aPTT), prothrombin time (PT), and thrombin time (TT). These methods allow measuring the time interval from the moment of adding a reagent (activator that triggers the clotting process) to the formation of a fibrin clot in the studied plasma.

The effect of $C_{60}(\text{OH})_{24}$ on plasma-coagulation hemostasis was assessed by adding it to plasma in the aPTT, PT, and TT tests. Five donors with normal PT, aPTT, and von Willebrand factor activity were selected.

The principle of the aPTT method is in the study of the plasma recalcification reaction under the conditions of standardization of the contact and phospholipid activation of blood coagulation. For this purpose, a contact activator (kaolin) and partial thromboplastin, which is functionally similar to platelet phospholipids, are added to the plasma. The sensitivity of this test to the deficiency of plasma-coagulation factors (excluding factors VII and XIII) is higher than in the test for determining the time of plasma recalcification, but standard phospholipid activation makes it impossible to detect the deficiency of the platelet coagulation activity. The determination of aPTT is a common method of monitoring heparin therapy.

The principle of the PT method consists of determining the clotting time of platelet-poor citrated plasma in the presence of an optimal amount of calcium and excess tissue thromboplastin. This is the variant of determining the time of plasma recalcification with the addition of tissue thromboplastin. In a complex with factor VII and Ca^{2+} , it directly activates factor X, so the test results depend on the activity of factor VII, factor X, and factors involved in the process of blood coagulation at the stages of thrombin and fibrin formation (factors V, II, and I).

The TT method is based on the ability of thrombin to induce the conversion of fibrinogen to fibrin without the participation of other blood coagulation factors, i.e., it allows to assess the final stage of blood coagulation (fibrinogen and its derivatives, the activity of factor XIII). Test elongation may indicate the presence of direct anticoagulants in the blood.

To determine aPTT, PT, and TT, we used the APTV-TEST, TEKHPLASTIN-TEST, and Thrombo-TEST reagent kits from Tekhnologiya-Standart, Russia. The studies were carried out using the APG2-02-P coagulometer (EKMO, Russia). A total of 50 μL of plasma and 50 μL of $C_{60}(\text{OH})_{24}$ solutions ($C = 10$, 50, 75, and 100 μM) were mixed, incubated at 37 °C for 60 s

and, in accordance with the study protocol, the clotting time was determined using an analyzer in the aPTT, PT, and TT tests.

2.3.4. Determination of NO-Radical Uptake. To determine the degree of NO-radical uptake, the Griess–Ilosvay reaction was used.⁴⁵ At physiological pH values, sodium nitroprusside is a donor of NO-radicals, the interaction of which with oxygen leads to the formation of NO_2^- . The nitrite anions formed as a result of the reaction can be detected using the Griess reagent (a pink-violet color of the solution is observed). For the experiment, the reaction mixture containing 1 mL of sodium nitroprusside ($C = 15 \mu\text{M}$) and 0.5 mL of the aqueous solution of fullereneol ($C = 10\text{--}200 \mu\text{M}$) was incubated in a shaker thermostat at 100°C . Then, 0.5 mL of PBS ($\text{pH} = 7.4$) and 0.5 mL of Griess reagent (0.1% solution in 20% acetic acid) were added to 0.25 mL of the resulting solution. The obtained mixture was incubated for 30 minutes at room temperature. The formed diazo compound was detected spectrophotometrically at $\lambda = 540 \text{ nm}$. Sodium azide was used as a positive control.

2.3.5. Determination of $C_{60}(\text{OH})_{24}$ Reducing Capacity. The reducing capacity of $C_{60}(\text{OH})_{24}$ was assessed by the ability of the fullereneol to reduce Fe^{3+} to Fe^{2+} .⁴⁶ The reaction mixture containing equal volumes (0.5 mL) of 0.1% potassium ferricyanide, phosphate buffer ($\text{pH} = 6.6$), and aqueous solutions of the fullereneol with various concentrations ($C = 500\text{--}1100 \mu\text{M}$) was incubated for 20 minutes in a water bath at 50°C . Then, 0.5 mL of trichloroacetic acid was added to the reaction mixture to terminate the reaction. After that, 1 mL of phosphate buffer ($\text{pH} = 6.6$) and 100 μL of FeCl_3 (0.1%) were added to 1 mL of the resulting solution. The mixture was left at room temperature for 10 minutes. The fullereneol caused the reduction of Fe^{3+} to Fe^{2+} because of its reductive capabilities according to the reaction: $\text{K}_3[\text{Fe}(\text{CN})_6] + \text{Reducing agent } (C_{60}(\text{OH})_{24}) = \text{Fe}(\text{CN})_6^{4-}$. A Prussian blue-colored complex is formed by adding FeCl_3 to Fe^{2+} : $\text{Fe}(\text{CN})_6^{4-} + \text{FeCl}_3 \rightarrow \text{Fe}_4[\text{Fe}(\text{CN})_6]_3$. Therefore, the reduction can be determined spectrophotometrically by measuring the formation of Perl's Prussian blue at 700 nm.⁴⁷ In this assay, the yellow color of the test solution changed to a blue color. Ascorbic acid was used as a positive control.

2.3.6. Photodynamic Properties. To study the photodynamic properties, the absorption spectra of the solutions were obtained: (i) Radachlorin; (ii) Radachlorin containing $C_{60}(\text{OH})_{24}$ in various concentrations; and (iii) Radachlorin in the presence of 500 μM sodium azide before and after irradiation with the red Laserland LED-2000 laser. The effect of $C_{60}(\text{OH})_{24}$ on the photobleaching of Radachlorin was evaluated using the photodegradation rate constant k_{deg} .^{44,48}

2.3.7. Human Platelet Aggregation. After obtaining informed consent, blood was taken for research from five donors, persons of both sexes aged 20–30, who did not receive drugs affecting platelet function for 7–10 days. To prevent platelet activation, blood was taken in vacuum tubes containing 3.8% sodium citrate ($C = 0.129 \text{ M}$) as a stabilizer in the ratio of sodium citrate to blood equal to 1:9. To obtain platelet-rich plasma, the stabilized blood was centrifuged at 1500 rpm for 10 min. Platelet aggregation in platelet-rich plasma was studied using the AP2110 SOLAR aggregometer (Belarus). ADP (final concentration of 10 μM) was used as an aggregation inducer. The plasma samples were incubated at 37°C before measurements. The aggregation was recorded before the curve reached a plateau.

2.3.8. Identification of the $C_{60}(\text{OH})_{24}$ Binding Sites at the HSA Molecule by Spectrofluorimetry. The binding of

$C_{60}(\text{OH})_{24}$ to HSA was studied using the Tecan Infinite M200 multimode microplate reader spectrofluorometer. The emission spectra were recorded in the wavelength range of 310–450 nm at 298.15 K; the excitation wavelength was 290 nm. The HSA concentration was 3 μM , the fullereneol concentration varied in the range $C = 0.3\text{--}1.5 \mu\text{M}$ with a 0.3 μM step and in the range $C = 6.0\text{--}24.0 \mu\text{M}$ with a 3.0 μM step. The measurements were carried out in the absence and presence of the following binding site markers: warfarin, ibuprofen, and digitonin with the final concentration of $C = 3 \mu\text{M}$.

2.3.9. Measuring the Binding Constants of the $C_{60}(\text{OH})_{24}$ –HSA Complex by the Thermal Shift Assay (TSA). Alternatively, the binding of $C_{60}(\text{OH})_{24}$ to HSA was estimated by TSA by measuring the melting point of pure HSA and after the addition of the ligand $C_{60}(\text{OH})_{24}$. Then, 25 μL of a mixture containing HSA ($C = 3 \mu\text{M}$), 0–100 μM of $C_{60}(\text{OH})_{24}$, and 200x ProteOrange fluorescent dye (Lumiprobe, Russia) was added to PCR tubes in triplicate.⁴⁹ The fluorescence data were acquired using the CFX96 Touch Real-Time PCR Instrument (Bio-Rad) with the excitation range of $\lambda = 470\text{--}533 \text{ nm}$. The temperature was held for 30 s per degree from 37 to 98°C ($\sim 0.5^\circ\text{C}\cdot\text{min}^{-1}$). The dependencies of the melting points on $C_{60}(\text{OH})_{24}$ concentrations were processed using GraphPad Prism 9.0.0 software, and the dissociation constants for the $C_{60}(\text{OH})_{24}$ –HSA complex were obtained by approximation.⁵⁰

2.3.10. Measurements of Esterase Activity. To study the effect of $C_{60}(\text{OH})_{24}$ on the esterase activity of HSA, the solutions of 4-nitrophenyl acetate (NPA) in ethanol (1 $\text{mg}\cdot\text{mL}^{-1}$) and HSA and fullereneol in phosphate buffer (PBS) with $\text{pH} = 7.02$ were prepared. After mixing the solutions, the final concentration of NPA was 100 μM , HSA was 3 μM , and the concentration of $C_{60}(\text{OH})_{24}$ varied from 0 to 24 μM . The rate of NPA hydrolysis was recorded by the formation of nitrophenol using the method of initial rates at 405 nm using a Tecan Infinite M200 multimode microplate reader spectrofluorometer.

2.3.11. $C_{60}(\text{OH})_{24}$ Binding to DNA. The binding of the $C_{60}(\text{OH})_{24}$ derivative to DNA was studied using the Tecan Infinite M200 multimode microplate reader spectrofluorometer. The DNA concentration was 2.5 μM ; the concentration range of $C_{60}(\text{OH})_{24}$ was $C = 3\text{--}45 \mu\text{M}$ in 3 μM increments. The solvent used was phosphate-buffered saline (PBS). The emission spectra were recorded in the 360–450 nm wavelength range at an excitation wavelength of 340 nm. The measurements were carried out at 303.15, 308.15, 313.15, and 318.15 K; the thermostat accuracy was $\Delta T = \pm 0.01 \text{ K}$. For calculations, the values of the fluorescence intensity at 380 nm were used.

2.3.12. Genotoxicity. The genotoxicity of $C_{60}(\text{OH})_{24}$ was evaluated using the method of DNA comets based on measuring the effect of $C_{60}(\text{OH})_{24}$ on the integrity of the DNA of human peripheral blood mononuclear cells (PBMC) using alkaline gel electrophoresis.⁵¹ The DNA comets were stained with the propidium iodide aqueous solution ($C = 10 \mu\text{g}\cdot\text{mL}^{-1}$) and visualized using a Micromed 3 LUM fluorescence microscope (Russia). The tail lengths were measured using CASP software (version 1.2.2). The DNA content in the tail and the tail length were determined experimentally; the tail moment was calculated as the percentage of DNA in the tail multiplied by the length between the center of the head and the tail.⁵²

2.3.13. Computer Simulation. MD simulations were performed using GROMACS 5 software suite;⁵³ the visualizations were made using the VMD program.⁵⁴ We chose the recent OPLS-AA/M force field,⁵⁵ which is the well-known OPLS-AA force field with improved protein parameters. The

potential model for HSA was obtained according to the protonation states corresponding to pH 7. The models for fullereneol isomers were built following the standard approach in the OPLS-AA force field. Namely, at the first step, the quantum-chemical geometry optimization was performed at the RHF/6-31G(d) level of theory. At the second step, the produced distribution of electrostatic potential was fitted with a set of point charges by means of the CHelpG algorithm. This procedure was performed for both uniform (random distribution of hydroxyl groups on the fullerene core surface) and “Saturn-like” (across the equatorial region of the fullerene core surface) isomers,³⁸ the R.E.D. server was used to facilitate the task.⁵⁶ For the hydroxyl groups, the atom types of diols were taken (atom types #169, #170). The carbon fullerene atoms were described with the parameters from the work of Girifalco,⁵⁷ while the rest of sp^2 -hybridized atoms were attributed with parameters for alkene C (atom type #141), and sp^3 -hybridized atoms were attributed with the atom type #159. The water model was TIP3P; for Na^+ and Cl^- ions, the default parameters were used.

The simulation cells were assembled according to the following procedure. The HSA molecule (in the crystallographic configuration) was solvated in a cubic water box with a side length equal to 10 nm containing $\sim 30\,000$ water molecules, and the neutralizing counter-ions and physiological saline were added, resulting in 96 Na^+ and 81 Cl^- ions. Then, the fullereneol molecule was placed at the docking sites DS1, DS2, or DS3 (Figure 1). The molecule appeared too large to fit in the sites in

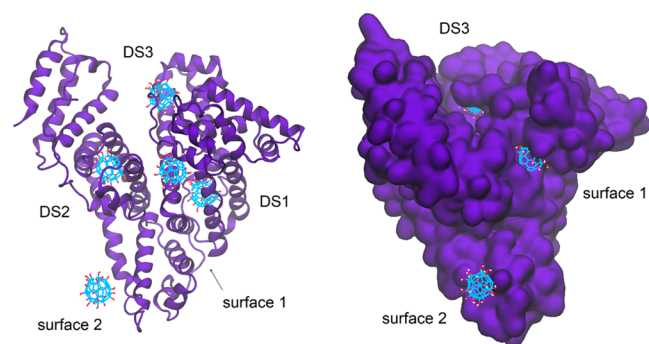


Figure 1. Positions of the $C_{60}(OH)_{24}$ molecule (the uniform isomer) in binding sites of HSA in the initial configurations for MD simulations.

the initial HSA configuration; therefore, an auxiliary simulation was necessary. Specifically, for each isomer in each docking site, a 500 ps slow-growth MD simulation was performed. In the initial state, the interactions between the fullereneol and HSA were zeroed, and they were gradually restored to the normal intensity during the calculation. The fullereneol was restrained in the initial location. As a result, six configurations of the fullereneol–HSA complex were obtained (Figure 2).

In addition to the above-mentioned configurations with fullereneol placed in the docking sites (DS1, DS2, or DS3), we also prepared two configurations where fullereneol isomers were located on the surface of the protein (Figure 1) following the same procedure. The first location was called “surface 1” further in the text, and it was in a fold of HSA; the second place was called “surface 2”, in which the fullereneol only made contact with HSA. These configurations were taken as initial for the productive MD runs of 20 ns long. The parameters were as follows: $T = 298.15$ K and $p = 1$ bar, velocity-rescale thermostat, Parrinello–Rahman barostat, 2 fs time step, the PME method

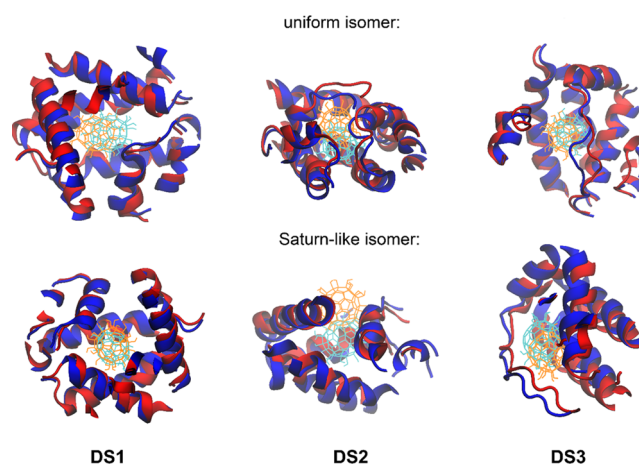


Figure 2. Displacement of the fullereneol $C_{60}(OH)_{24}$ after 20 ns of MD simulation. The initial configurations (at 0 ns) are colored in red and orange, the final ones (at 20 ns) are colored in blue. The two configurations are fitted to minimize the root-mean-square displacement of the docking site, not the whole protein, between 0 and 20 ns. Only 1–1.5 nm vicinity of the fullereneol is shown for clarity. The view direction is chosen to maximally show all of the magnitudes of the fullereneol displacement.

for electrostatic interactions, 1 nm cut-off of van der Waals interactions, constraints on all bonds.

2.4. Statistics Analysis. All calculations were performed using Origin software (Origin Lab Corporation, Northampton, Massachusetts). P-values were considered significant at 0.05, 0.01, and 0.001. Data were analyzed using Student’s t-test. Physicochemical experiments were carried out three times. All biological experiments were repeated eight times. All data are presented as mean \pm standard error of the mean (SEM).

3. RESULTS AND DISCUSSION

3.1. Effect of $C_{60}(OH)_{24}$ on Spontaneous Erythrocyte Hemolysis. To assess the biocompatibility of $C_{60}(OH)_{24}$, its effect on the spontaneous erythrocyte hemolysis was studied. In the case of substances compatible with blood, the erythrocyte membrane remains intact, and the content of the cell is not released. In our case, the toxicity of $C_{60}(OH)_{24}$ was determined by evaluating the released hemoglobin. Figure 3 shows that $C_{60}(OH)_{24}$, when incubated for 1 and 3 h, caused very mild hemolysis in the whole concentration range; the rate of hemolysis was dose- and time-dependent. It is generally accepted that the nanomaterials are classified as nonhemolytic if the hemolysis rate does not exceed 5%.⁵⁸ Consequently, fullereneol $C_{60}(OH)_{24}$ can be considered safe in concentrations up to 100 μM .

3.2. Evaluation of $C_{60}(OH)_{24}$ Anti-/Pro-Oxidant Properties. It is known that erythrocyte lysis is initiated by irradiation with ultraviolet or visible light in the presence of photosensitizers, the most effective of which are porphyrins and their derivatives,⁵⁹ in particular Radachlorin. It was found that the photodynamic effect is primarily due to the generation of singlet oxygen and other ROS. The binding of porphyrins to cell membranes leads to the decrease of the photostability of membranes.⁷

Figure 4 shows the dependence of TC_{50} on the concentration of $C_{60}(OH)_{24}$. As can be seen from the obtained results, $C_{60}(OH)_{24}$ was statistically significant, in comparison with the control, inhibited hemolysis induced by Radachlorin, which was

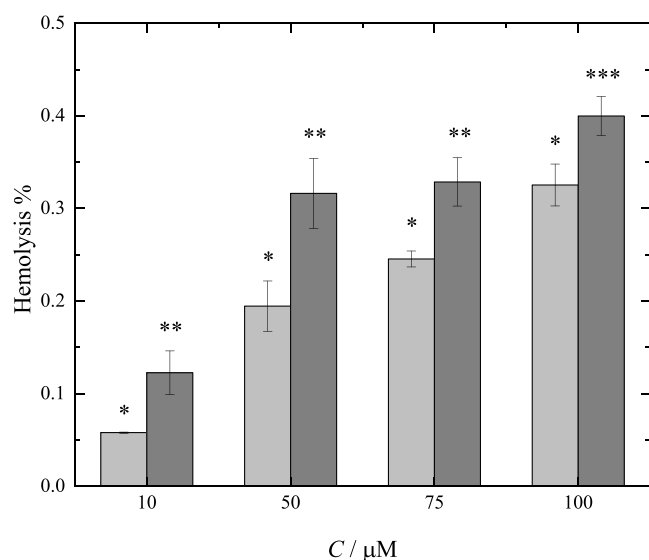


Figure 3. Effect of $C_{60}(\text{OH})_{24}$ on the degree of erythrocyte hemolysis after 1 h (light gray) and 3 h (dark gray) of incubation. C is the molar concentration of $C_{60}(\text{OH})_{24}$. * $p < 0.05$ relative to control (1 h). ** $p < 0.05$ relative to negative control (3 h). *** $p < 0.01$ relative to control (3 h).

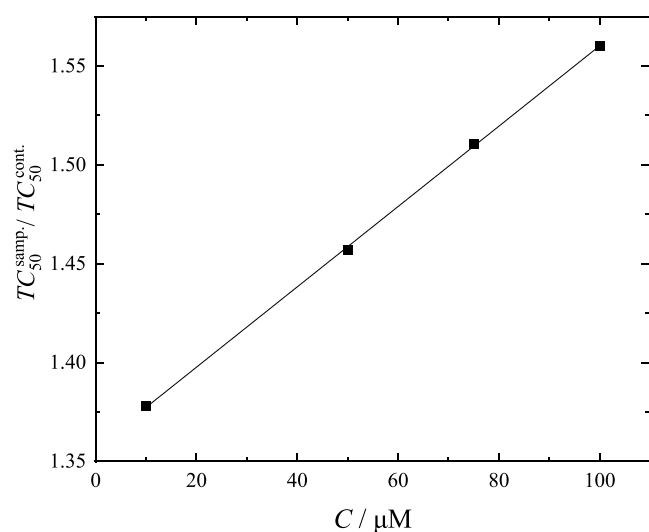


Figure 4. Concentration dependence of the degree of photo-induced hemolysis in the presence of $C_{60}(\text{OH})_{24}$. C is the molar concentration of fullereneol, $\text{TC}_{50}^{\text{smp.}}$ is the time of photo-induced hemolysis of 50% of erythrocytes in the presence of $C_{60}(\text{OH})_{24}$, and $\text{TC}_{50}^{\text{cont.}}$ is the time of photo-induced hemolysis of 50% of erythrocytes in the presence of physiological saline (control).

manifested in the increase of the hemolysis time of 50% of erythrocytes (TC_{50}). It can be concluded that $C_{60}(\text{OH})_{24}$ exhibits dose-dependent antioxidant activity.

3.3. Effect of $C_{60}(\text{OH})_{24}$ on Coagulation Hemostasis. As can be seen from the data presented in Table 3, $C_{60}(\text{OH})_{24}$ at the concentrations of 50–100 μM leads to a statistically significant increase in PT and TT in the blood of healthy donors compared to the control. An increase in aPTT is observed at all studied concentrations of the fullereneol. Thus, $C_{60}(\text{OH})_{24}$ exhibits pronounced anticoagulant properties in the studied concentration range ($C = 10\text{--}100 \mu\text{M}$).

3.4. NO-Radical Uptake. NO-radical is an important chemical mediator generated by endothelial cells, macrophages, and neurons and involved in the regulation of various physiological processes. Excess concentration of NO-radical uptake provokes cytotoxic effects during various disorders such as AIDS, cancer, Alzheimer's disease, and arthritis. The oxygen reacts with the excess of NO-radical uptake to generate nitrite and peroxynitrite anions, which act as free radicals.

From Figure 5, it can be seen that fullereneol reacts with the NO-radical in the entire concentration range ($C = 10\text{--}200 \mu\text{M}$),

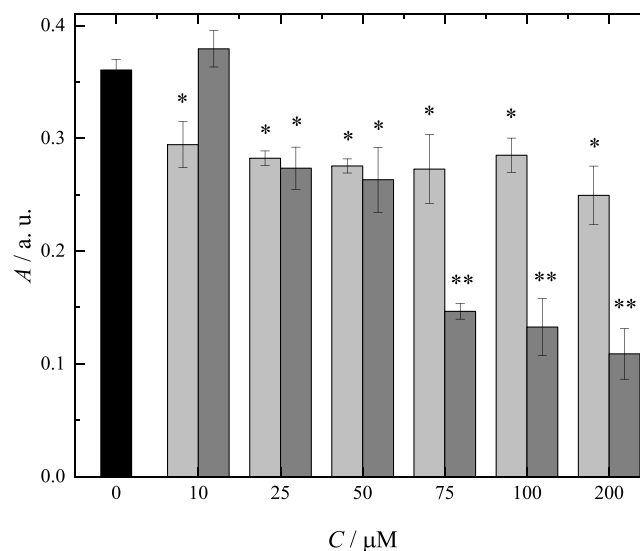


Figure 5. Effect of $C_{60}(\text{OH})_{24}$ (light gray) and sodium azide (dark gray) on NO-radical uptake. * $p < 0.05$ relative to control. ** $p < 0.01$ relative to control.

although its antiradical activity is less pronounced compared to sodium azide. We can conclude that fullereneol is a weak NO-radical scavenger, and it is impossible to evaluate the IC_{50} value. At the same time, previously, we obtained experimental data on the kinetics of the interaction of $C_{60}(\text{OH})_{22\text{--}24}$ with the DPPH radical and determined moderate antiradical activity of fullereneol.⁴⁰ The results obtained are in good agreement with

Table 3. Indicators of Coagulation Hemostasis Following the Addition of $C_{60}(\text{OH})_{24}$ to Human Plasma

| test type | standard | control | C (μM) | | | |
|-----------|----------|----------------|-----------------------------|-----------------------------|-----------------------------|-----------------------------|
| | | | 10 | 50 | 75 | 100 |
| | | | coagulation time (s) | | | |
| TT (s) | 15–19 | 17.1 \pm 1.6 | 16.2 \pm 1.3 | 40 \pm 1.2 ^a | 42.6 \pm 1.8 ^a | >120.0 |
| aPTT (s) | 28–40 | 36.5 \pm 1.9 | 46.3 \pm 0.9 ^a | 65.2 \pm 0.8 ^a | 66.8 \pm 0.7 ^a | 68.4 \pm 1.6 ^a |
| PT (s) | 13–18 | 13.6 \pm 1.8 | 15.0 \pm 1.0 | 16.5 \pm 1.3 ^a | 21.2 \pm 1.5 ^a | 20.1 \pm 1.2 ^a |

^a $p < 0.05$ relative to control.

previously published work on the antioxidant properties of polyhydroxylated fullerenes with various contents of hydroxyl groups.^{60–63}

3.5. Reducing Capacity of $C_{60}(OH)_{24}$. It can be seen from the graph presented in Figure 6 that fulleranol exhibits the

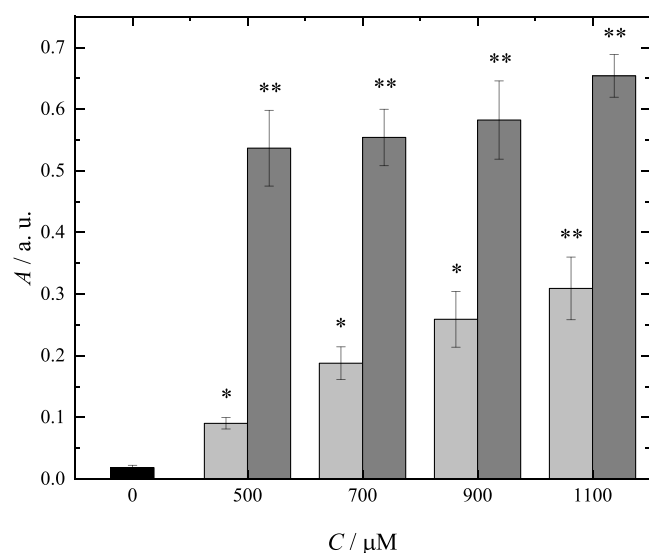


Figure 6. Reducing capacity of $C_{60}(OH)_{24}$ (light gray) and ascorbic acid (dark gray). * $p < 0.05$ relative to control. ** $p < 0.01$ relative to control.

properties of a reducing agent in the entire concentration range ($C = 500–1100 \mu\text{M}$), although the reducing capacity is less pronounced compared to ascorbic acid. The reducing capacity of fulleranol is dose dependent. Fe^{3+} reduction is often used as an indicator of the electron-donating activity, which is potentially important for determining the fulleranol action mechanism. The reducing capacity is associated with the antioxidant potential of fulleranol. In our case, the results of NO-radical uptake and reducing capacity methods are in good agreement: fulleranol possesses low antiradical activity against NO-radicals and, at the same time, a moderate activity in the electron-donating reaction with Fe^{3+} . Thus, the results obtained are in good agreement with the data of ref 9.

3.6. Photobleaching. The photosensitizer degradation was evaluated by measuring the photodegradation rate constants, the values of which were determined as the slope of the kinetic curves in the coordinates $\ln(A_t/A_0) - t$. The decrease in k_{deg} indicates the presence of singlet oxygen quencher properties of the test compound. In turn, the increase in k_{deg} indicates that the test compound has the properties of a singlet oxygen inducer.

Radachlorin absorption spectra were measured in the absence and in the presence of various concentrations of $C_{60}(OH)_{24}$ ($C = 10, 50, 75, 100 \mu\text{M}$). The solution of sodium azide ($C = 500 \mu\text{M}$), which is a strong antioxidant, was used as a control. As an example, the absorption spectra of Radachlorin in the presence of $C_{60}(OH)_{24}$ ($C = 2.5 \text{ mg}\cdot\text{L}^{-1}$), in the absence, and under irradiation (10–50 s) are shown in Figure 7. Based on the obtained spectra with various fulleranol content, the dependences of $\ln(A_t/A_0)$ on the irradiation time were plotted. Figure 8 and Table 4 reveal that the addition of $C_{60}(OH)_{24}$ to Radachlorin leads to a decrease in k_{deg} . Thus, it can be stated that $C_{60}(OH)_{24}$ exhibits dose-dependent antioxidant properties.

3.7. Human Platelet Aggregation. Table 5 shows the results of measuring the effect of $C_{60}(OH)_{24}$ on human platelet

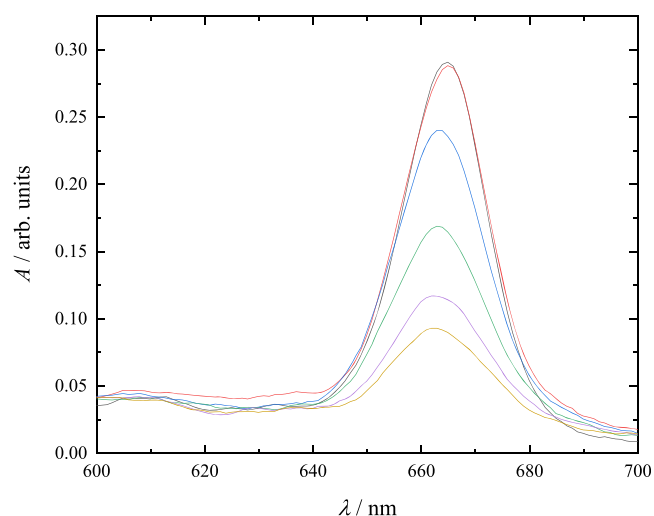


Figure 7. Absorption spectra of Radachlorin + $C_{60}(OH)_{24}$ ($C = 2.5 \text{ mg}\cdot\text{L}^{-1}$) without irradiation (—) and under irradiation (red line, 10 s; blue line, 20 s; green line, 30 s; purple line, 40 s; orange line, 50 s).

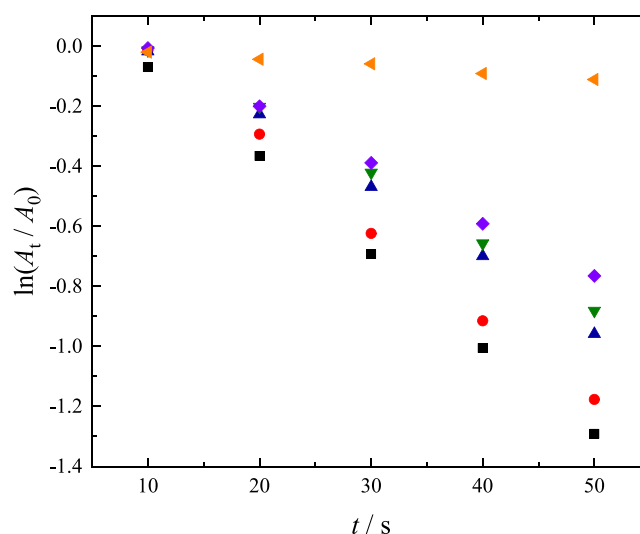


Figure 8. Kinetic dependence of photobleaching of Radachlorin (■) in the presence of $C_{60}(OH)_{24}$ (red circle solid, 10 μM ; blue triangle up solid, 50 μM ; green triangle down solid, 75 μM ; purple titled square solid, 100 μM) and NaN_3 (orange triangle left-pointing solid, 500 μM). A_t and A_0 are the optical densities of Radachlorin solutions at 659 nm before and after irradiation.

Table 4. Values of the Photobleaching Constant of Radachlorin in the Presence of NaN_3 and $C_{60}(OH)_{24}$

| agent | C (μM) | K_{deg} (s^{-1}) |
|-------------------|-----------------------|--------------------------------------|
| $C_{60}(OH)_{24}$ | 10 | 0.0308 ± 0.0004 |
| $C_{60}(OH)_{24}$ | 50 | 0.0295 ± 0.0006 |
| $C_{60}(OH)_{24}$ | 75 | 0.0235 ± 0.0005 |
| $C_{60}(OH)_{24}$ | 100 | 0.0219 ± 0.0005 |
| $C_{60}(OH)_{24}$ | 100 | 0.0191 ± 0.0002 |
| NaN_3 | 500 | 0.0023 ± 0.0001 |

aggregation in the presence of the platelet aggregation inducer (ADP). It can be concluded that $C_{60}(OH)_{24}$ in the concentration range $C = 10–50 \mu\text{M}$ does not affect platelet aggregation, and a further increase in the concentration of $C_{60}(OH)_{24}$ leads to the decrease in aggregation compared to the

Table 5. Effect of $C_{60}(OH)_{24}$ on Platelet Aggregation in the Presence of ADP

| control | amplitude (%) | | | |
|-----------------|--|------------------|-------------------------------|------------------------------|
| | concentration of $C_{60}(OH)_{24}$ (μM) | | | |
| | 10 | 50 | 75 | 100 |
| 83.4 \pm 7.32 | 77.50 \pm 4.16 | 76.57 \pm 5.28 | 56.87 \pm 5.28 ^a | 59.5 \pm 5.91 ^a |

^a $p < 0.05$ relative to control.

control group. Thus, $C_{60}(OH)_{24}$ has antiplatelet activity at $C > 50 \mu M$ in tests for ADP-induced platelet aggregation.

3.8. Binding of $C_{60}(OH)_{24}$ to HSA by Spectrofluorimetric Data. Albumin has three main ligand-binding sites: (i) site I, located in the subdomain IIA (warfarin binding site); (ii) site II, located in the subdomain IIIA (ibuprofen binding site); and (iii) site II located in the subdomain IB (digitonin binding site).⁶⁴ To identify the binding sites of $C_{60}(OH)_{24}$ to HSA, competitive binding experiments were performed in the presence of binding site markers. To determine the binding constants (K_b), as well as the stoichiometry of the binding reaction (n), the Scatchard equation was used

$$\lg \frac{F_0 - F}{F} = \lg K_b + n \lg Q \quad (2)$$

where F_0 is the HSA fluorescence intensity in the absence of $C_{60}(OH)_{24}$, F is the HSA fluorescence intensity in the presence of $C_{60}(OH)_{24}$, and Q is the molar concentration of $C_{60}(OH)_{24}$.

It is important to take into account the inner-filter effect, resulting in the additional quenching of fluorescence caused by the absorption of excitation and emission radiation. This phenomenon may not be considered in our system due to low absorbance.

Figure 9 presents data on the binding of HSA to $C_{60}(OH)_{24}$ in Hill coordinates ($\lg \frac{F_0 - F}{F}$ vs $\lg Q$). The obtained dependence has an inflection point, which corresponds to the presence of two binding sites.⁶⁵ In the concentration range $C = 3 \times 10^{-7} - 1.5 \times 10^{-6}$ M, binding to the first site occurs, and in the concentration range $C = 6.0 \times 10^{-6} - 2.4 \times 10^{-5}$ M binding to the second one

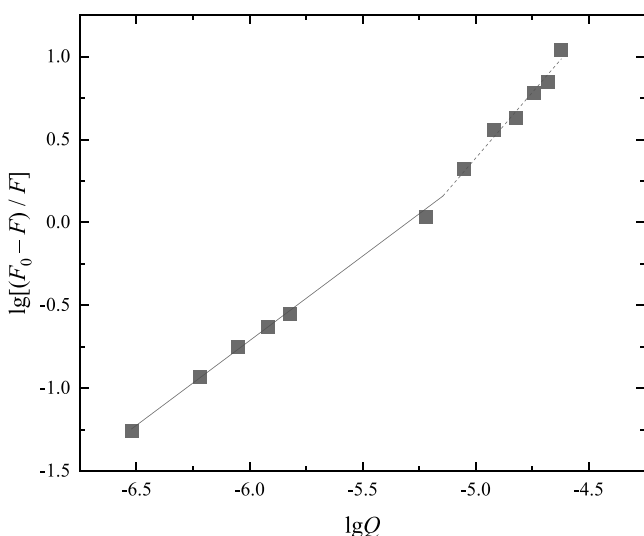


Figure 9. Dependence of the binding process of $C_{60}(OH)_{24}$ to HSA at 298.15 K in the absence of binding site markers in Hill coordinates. F_0 is the HSA fluorescence intensity in the absence of $C_{60}(OH)_{24}$, F is the HSA fluorescence intensity in the presence of $C_{60}(OH)_{24}$, and Q is the molar concentration of $C_{60}(OH)_{24}$.

takes place. In Table S1 (Supporting Information), the data on the binding of HSA to $C_{60}(OH)_{24}$ with markers (warfarin, ibuprofen, digitonin) are presented in Hill coordinates. Table 6

Table 6. Logarithms of the Binding Constants ($\lg K_b$) and the Stoichiometry of the Binding Reaction (n) of $C_{60}(OH)_{24}$ to HSA

| site marker | $C = 3 \times 10^{-7} - 1.5 \times 10^{-6}$ M | | $C = 6 \times 10^{-6} - 2.4 \times 10^{-5}$ M | |
|-------------|---|-----------------|---|-----------------|
| | $\lg K_b$ ($\lg M^{-1}$) | n | $\lg K_b$ ($\lg M^{-1}$) | n |
| no markers | 5.4 \pm 0.2 | 1.02 \pm 0.03 | 2.9 \pm 0.2 | 0.56 \pm 0.03 |
| warfarin | 5.2 \pm 0.2 | 0.97 \pm 0.03 | 3.3 \pm 0.2 | 0.61 \pm 0.04 |
| ibuprofen | 5.1 \pm 0.2 | 0.95 \pm 0.04 | 1.0 \pm 0.1 | 0.15 \pm 0.02 |
| digitonin | 4.5 \pm 0.3 | 0.88 \pm 0.05 | 3.0 \pm 0.3 | 0.52 \pm 0.04 |

demonstrates the data on the stoichiometry of the binding of HSA to $C_{60}(OH)_{24}$ (n), as well as the logarithm of the binding constants in the presence and absence of markers (warfarin, ibuprofen, digitonin) for two concentration ranges $C = 3 \times 10^{-7} - 1.5 \times 10^{-6}$ and $6.0 \times 10^{-6} - 2.4 \times 10^{-5}$ M.

From the obtained data, it is seen that (i) the values of $\lg K_b$ and n do not change in both concentration ranges with the addition of warfarin; (ii) in the concentration range $C = 3 \times 10^{-7} - 1.5 \times 10^{-6}$ M, the decrease in $\lg K_b$ and n is observed with the addition of digitonin; (iii) in the concentration range $C = 6.0 \times 10^{-6} - 2.4 \times 10^{-5}$ M, the decrease in $\lg K_b$ and n is observed with the addition of ibuprofen. Based on the values of the binding constants ($K_b = 2.51 \pm 0.09 \times 10^5 M^{-1}$ for the first concentration site and $7.9 \pm 0.5 \times 10^2 M^{-1}$ for the second one), $C_{60}(OH)_{24}$ forms a strong complex with HSA in the subdomain IB and it weakly binds in the subdomain IIIA.

3.9. Binding to HSA by TSA Data. To determine the dissociation constants, we applied an approach described in refs 49, 50. The experimental data on the fluorescence vs temperature (a) and its first derivative (b) are presented in Figure 10. The obtained results on the HSA melting point vs fullerene concentration are demonstrated in Figure 11. The concentration dependence of the melting point can be clearly divided into two parts: the concentration ranges $C = (0 - 1.6) \times 10^{-6}$ and $3.13 \times 10^{-6} - 10^{-4}$ M corresponding to the digitonin and ibuprofen binding sites of HSA (see Section 3.8). To obtain the values of the dissociation constants for both concentration ranges, the data were processed using the following equation

$$t = \frac{B_{\max} \cdot C}{K_d + C} + NS \cdot C + B \quad (3)$$

where t is the melting point of the $C_{60}(OH)_{24}$ -HSA complex, B_{\max} is the maximum binding (units of temperature), C is the fullerene concentration, K_d is the dissociation constant (units of concentration), NS is the slope of a nonlinear regression (units of temperature divided by units of concentration), and B is the measured binding with no ligand added. The correlation parameters are shown in Table 7.

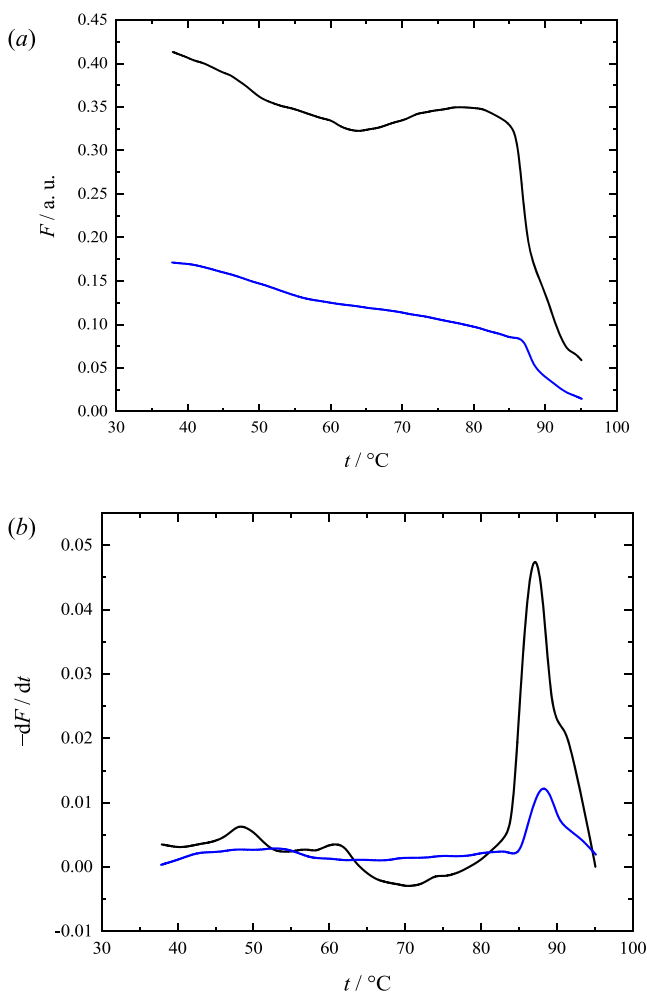


Figure 10. Temperature dependence of fluorescence (a) and its first derivative (b) for the $C_{60}(\text{OH})_{24}$ -HSA complex (blue line, $C = 10^{-4}$ M) in comparison to pure HSA (black line).

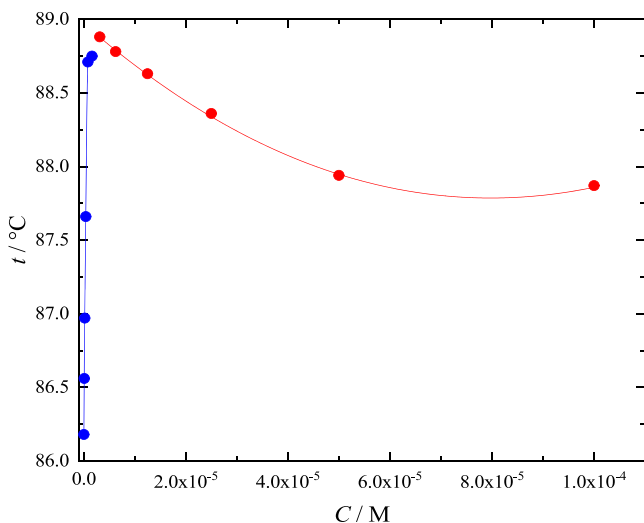


Figure 11. Dependence of fullereneol concentration on the $C_{60}(\text{OH})_{24}$ -HSA complex melting point.

As a result (Figure 12), the following values of the binding constants (reciprocals of the dissociation constants) were retrieved: $2.28 \times 10^5 \pm 0.07 \text{ M}^{-1}$ ($C = 0-1.6 \times 10^{-6}$ M) and $4.56 \times 10^2 \pm 0.03 \text{ M}^{-1}$ ($C = 3.13 \times 10^{-6}-10^{-4}$ M), which is in

Table 7. Correlation Parameters of eq 3 Applied for Determining the Dissociation Constant of the $C_{60}(\text{OH})_{24}$ -HSA Complex

| parameter | $C = 0-1.6 \times 10^{-6}$ M | $C = 3.13 \times 10^{-6}-10^{-4}$ M |
|---|------------------------------|-------------------------------------|
| B_{max} ($^\circ\text{C}$) | 3866 | -962.3 |
| NS ($^\circ\text{C} \cdot \text{M}^{-1}$) | -83 253 674 | 408 375 |
| B ($^\circ\text{C}$) | 86.13 | 88.97 |

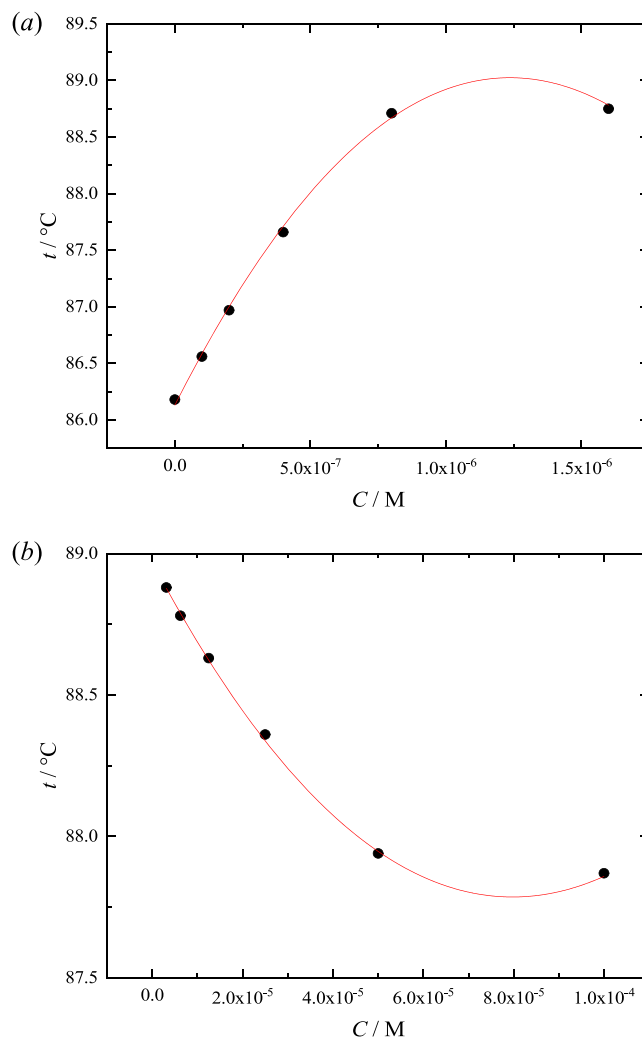


Figure 12. Concentration dependence of the melting point of the $C_{60}(\text{OH})_{24}$ -HSA complex in the concentration ranges $C = 0-1.6 \times 10^{-6}$ M (binding to digitonin, a) and $C = 3.13 \times 10^{-6}-10^{-4}$ M (binding to ibuprofen, b). Dots are experimental values; lines represent the approximation by eq 3.

good correspondence with the data obtained by spectrofluorimetry.

3.10. Esterase Activity. To determine the rate constant of the NPA hydrolysis reaction, the first-order reaction equation was used

$$\ln \left(1 - \frac{A_t - A_0}{A_{\text{NF}}} \right) = -kt \quad (4)$$

where $A_{\text{NF}} = 1.86$ (the optical density of the nitrophenol solution with $100 \mu\text{M}$ concentration); A_t is the optical density of the reaction mixture at time t ; A_0 is the optical density of the reaction mixture at the initial time; k is the reaction rate constant

(min^{-1}); and t is the time from the beginning of the reaction (min).

The kinetic dependences of the reaction of NPA hydrolysis with HSA in the absence and presence of $\text{C}_{60}(\text{OH})_{24}$ were obtained. As an example, Figure 13 shows the kinetic dependences of the reaction of NPA hydrolysis with HSA in the absence and presence of $24 \mu\text{M}$ $\text{C}_{60}(\text{OH})_{24}$.

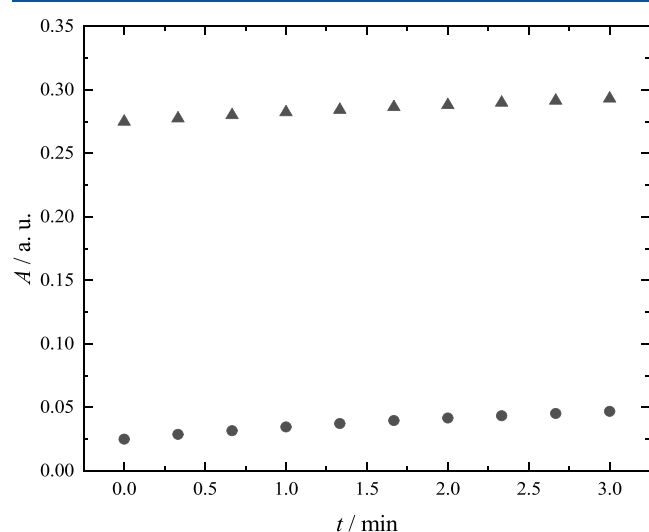


Figure 13. Kinetic dependences of the hydrolysis reaction of NPA with HSA in the absence (●) and presence of $24 \mu\text{M}$ $\text{C}_{60}(\text{OH})_{24}$ (▲).

Furthermore, based on the data on the change in optical density, the dependences were plotted in the coordinates $\ln\left(1 - \frac{A_t - A_0}{A_{\text{NF}}}\right)$ vs t . As an example, Figure 14 presents the data for the hydrolysis reaction of NPA with HSA in the absence and presence of $24 \mu\text{M}$ $\text{C}_{60}(\text{OH})_{24}$.

The first-order reaction rate constants were determined as the slope of the dependence of $\ln\left(1 - \frac{A_t - A_0}{A_{\text{NF}}}\right)$ on t (Figure 15). From Figure 15, it can be seen that $\text{C}_{60}(\text{OH})_{24}$ in the

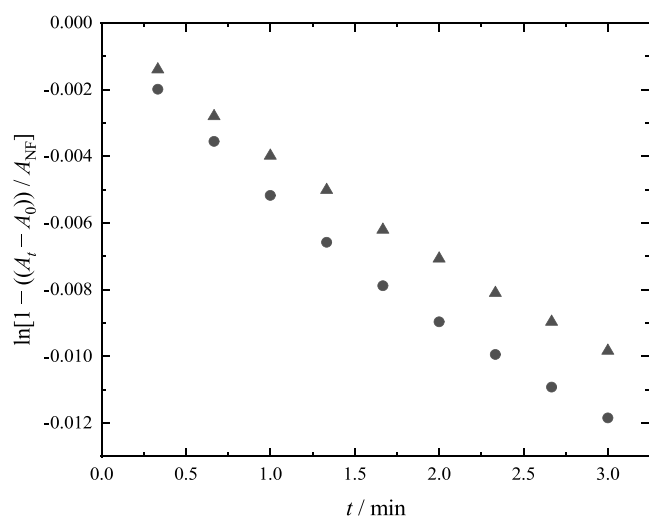


Figure 14. Dependencies $\ln\left(1 - \frac{A_t - A_0}{A_{\text{NF}}}\right)$ on time for the reaction of hydrolysis of NPA with HSA in the absence (●) and in the presence of $24 \mu\text{M}$ $\text{C}_{60}(\text{OH})_{24}$ (▲).

concentration range $2.4\text{--}24 \mu\text{M}$ partially inhibits the esterase activity of HSA.

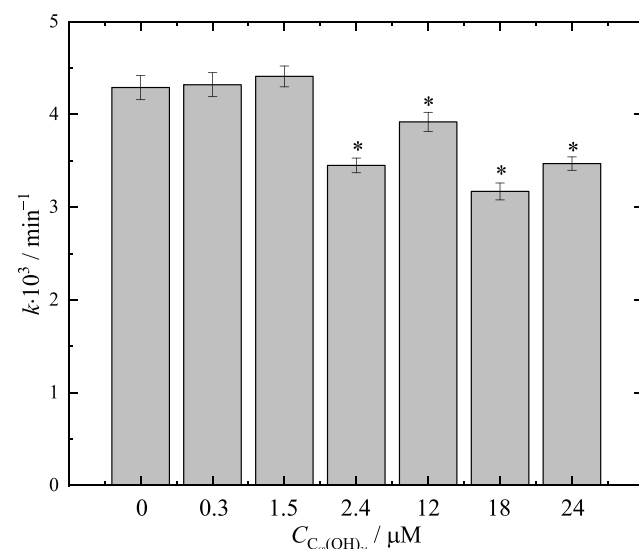


Figure 15. Values of the rate constants of the hydrolysis reaction of NPA with HSA in the concentration range of $\text{C}_{60}(\text{OH})_{24}$ $0\text{--}24 \mu\text{M}$. * $p < 0.05$ relative to control (in the absence of $\text{C}_{60}(\text{OH})_{24}$).

3.11. $\text{C}_{60}(\text{OH})_{24}$ Binding to DNA. Figure 16 demonstrates the DNA fluorescence spectra in the absence and presence of

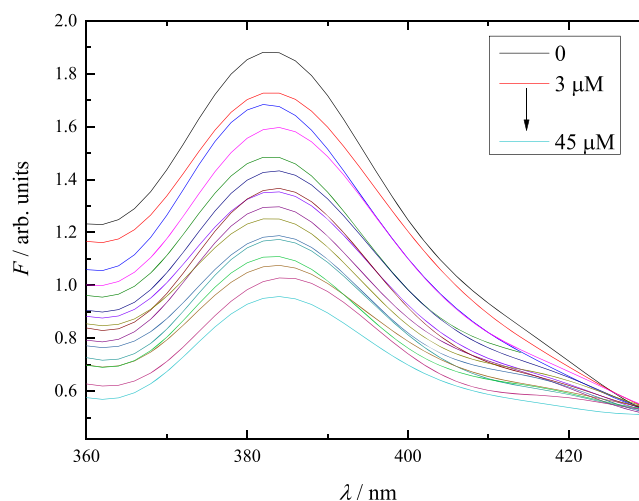


Figure 16. DNA fluorescence spectra in the absence and presence of $\text{C}_{60}(\text{OH})_{24}$ ($C = 3\text{--}45 \mu\text{M}$) at 303.15 K .

$\text{C}_{60}(\text{OH})_{24}$ at 298.15 K . To determine the binding constants (K_b), as well as the stoichiometry of the binding reaction (n), the Scatchard equation was used (see eq 2). For this, the experimental dependences were plotted in Hill coordinates. Figure 17 shows an example of the dependence in Hill coordinates at 303.15 K . The calculated values of K_b and n are presented in Table 8. The order of the obtained K_b values in the temperature range $T = 303.15\text{--}318.15 \text{ K}$ ($10^3\text{--}10^4 \text{ M}^{-1}$) indicates the formation of strong $\text{C}_{60}(\text{OH})_{24}$ complexes with DNA. The changes in the enthalpy and entropy of the reaction of $\text{C}_{60}(\text{OH})_{24}$ binding to DNA were calculated using the van't Hoff equation neglecting the influence of temperature

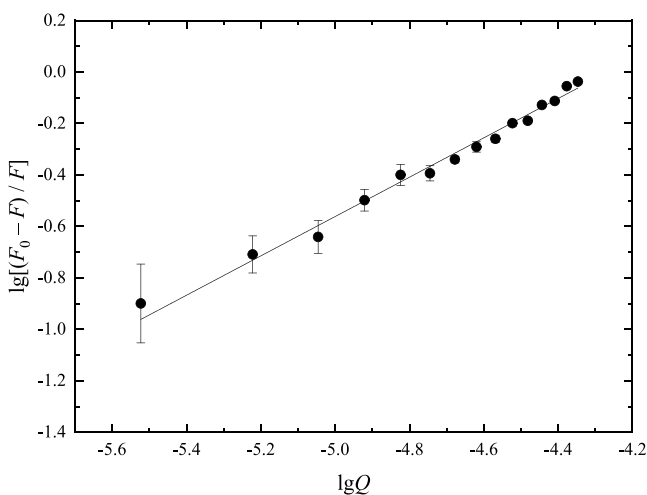


Figure 17. Dependence of the $C_{60}(OH)_{24}$ binding process to DNA at 303.15 K in Hill coordinates.

$$\ln K_b = -\frac{\Delta H}{RT} + \frac{\Delta S}{R} \quad (5)$$

where ΔH and ΔS are the changes in the enthalpy and the entropy of the reactions of $C_{60}(OH)_{24}$ binding to DNA, respectively, R is the gas constant, and T is the absolute temperature.

The changes in the Gibbs energy (ΔG) of the reaction of $C_{60}(OH)_{24}$ binding to DNA in the temperature range 303.15–318.15 K was calculated using the following equation

$$\Delta G = \Delta H - T\Delta S \quad (6)$$

Negative ΔG values in the temperature range 303.15–318.15 K indicate that the binding process of the $C_{60}(OH)_{24}$ derivative to DNA is thermodynamically favorable. Positive values of ΔH and ΔS are typical of hydrophobic interactions; therefore, it can be assumed that the formation of $C_{60}(OH)_{24}$ complexes with DNA occurs due to the fullerene core. In ref 66, the authors showed that fullereneol $C_{60}(OH)_{24}$ interacts with the phosphate backbone of the outer side of the native DNA double helix, as well as with pairs of nitrogenous bases inside the major groove of DNA. Comparison of K_b shows that the values obtained in ref 66 exceed the K_b values obtained in this study by one to two orders of magnitude. This fact is due to the different temperature ranges in which the binding study was carried out, as well as due to the fact that different methods were used to obtain fullerenols and, as a consequence, the synthesized adducts had different compositions. For example, it was shown by solid-state ^{13}C NMR spectroscopy that the fullereneol used in our study contains a small amount of epoxy groups.

3.12. Genotoxicity Results. The average values of % tail DNA, the tail length, and the tail moment of comets observed for human PBMCs incubated in the presence of H_2O_2 (positive control), phosphate-saline buffer (negative control), and

$C_{60}(OH)_{24}$ are presented in Table 9. It can be seen that the amount of DNA damage in the presence of H_2O_2 is significantly higher than that of control cells. As an example, Figure 18 presents the photographs of the DNA comets in the presence of H_2O_2 ($C = 3.4 \mu g \cdot L^{-1}$), the phosphate-saline buffer, and $C_{60}(OH)_{24}$ ($C = 10, 50, 75,$ and $100 \mu M$). It can be concluded that $C_{60}(OH)_{24}$ possesses moderate dose-dependent genotoxicity. Based on the study of the frequencies of micronucleus formation and chromosomal aberrations, the authors of refs 20, 67 showed that fullereneol $C_{60}(OH)_{24}$ does not cause significant genotoxic effects to CHO-K1 cells (Chinese hamster ovary cells K1) and human peripheral blood monocytes, and also established its projective effect when cells are exposed to the alkylating agent Mitomycin C.

3.13. Computer Simulation. The analysis of the MD simulation results showed that both uniform and Saturn-like isomers are strongly bound in the docking sites. During the 20 ns of simulations, the molecules remained in the initial locations or close to them (Figure 2). This can be explained by the buried location of the molecule, which demands considerable deformation of the protein for the fullereneol to desorb, and the presence of hydrogen bonds between the constituents. The average number of hydrogen bonds is listed in Table 10, and the time evolution is depicted in Figure 19. The isomers show similar behavior, except for the DS2 site, where the Saturn-like isomer forms approximately two times more hydrogen bonds with HSA.

The results of the simulations started from the initial configurations with fullereneol located near the HSA surface shed more light on the importance of the $C_{60}(OH)_{24}$ –HSA hydrogen bonding. In the case when the fullereneol molecule was placed in a fold (“surface 1”), it remained in that place being held by hydrogen bonds. On the contrary, when the uniform isomer was placed at the other location (“surface 2”) that did not provide sufficient hydrogen bonding, it desorbed and remained in the solution except at the interval (12–20 ns) when it was adsorbed on the surface being bound with 2.7 hydrogen bonds in average. The Saturn-like isomer in the same position (“surface 2”) managed to form more hydrogen bonds with the surface (~ 3.6), which allowed it to stay near the initial position during all 20 ns of the calculations. This indicates that for strong binding, abundant hydrogen bonding with HSA is needed. Also, the binding is seen to occur not only in the specific docking sites but on the surface, as well.

Finally, examining the initial configurations makes it clear that at experimental conditions, the fullereneol molecules are unable to reach the DS1 site compared to more reachable DS2 and DS3 sites.

4. CONCLUSIONS

We present the experimental data on the biocompatibility of aqueous solutions of well-defined fullereneol $C_{60}(OH)_{24}$, namely, its cyto- and genotoxicity, spontaneous and photo-induced

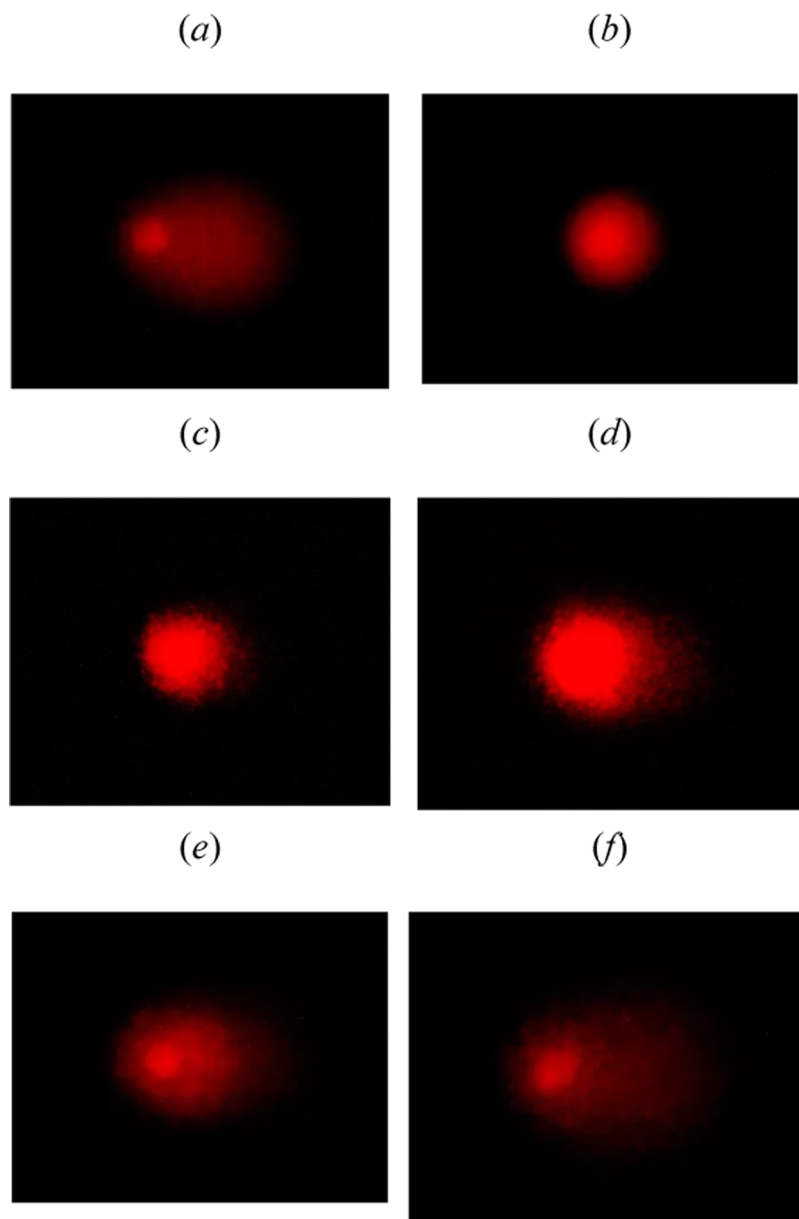
Table 8. Thermodynamic Parameters of the $C_{60}(OH)_{24}$ Binding to DNA and the Number of Binding Sites in the Temperature Range 303.15–318.15 K

| T (K) | n | $K_b \times 10^3$ (M^{-1}) | ΔG ($kJ \cdot mol^{-1}$) | ΔH ($kJ \cdot mol^{-1}$) | ΔS ($J \cdot K^{-1} \cdot mol^{-1}$) |
|---------|-------------|--------------------------------|------------------------------------|------------------------------------|--|
| 303.15 | 0.76 ± 0.04 | 1.8 ± 0.1 | −19.0 ± 3.2 | 115 ± 15 | 443 ± 46 |
| 308.15 | 0.86 ± 0.04 | 4.8 ± 0.3 | −21.3 ± 3.5 | | |
| 313.15 | 0.89 ± 0.03 | 6.7 ± 0.3 | −23.5 ± 3.9 | | |
| 318.15 | 0.98 ± 0.07 | 17.9 ± 1.4 | −25.7 ± 4.3 | | |

Table 9. Effect of $C_{60}(OH)_{24}$ on % Tail DNA, Tail Length, and Tail Moment

| characteristic studied | negative control | concentration of H_2O_2 (μM) | amplitude (%) | | | |
|------------------------|------------------|---------------------------------------|--|--------------------|--------------------|--------------------|
| | | | concentration of $C_{60}(OH)_{24}$ (μM) | | | |
| | | 100.0 | 10.0 | 50.0 | 75.0 | 100.0 |
| % tail DNA | 0.84 ± 0.38 | 82.14 ± 2.03^c | 5.70 ± 1.85^b | 13.18 ± 3.26^b | 17.84 ± 2.60^b | 22.47 ± 3.50^b |
| tail length | 28.59 ± 4.27 | 646.63 ± 67.67^b | 15.08 ± 3.81 | 25.08 ± 4.51 | 31.10 ± 6.93 | 25.25 ± 5.95 |
| tail moment | 0.24 ± 0.08 | 531.14 ± 19.89^c | 0.85 ± 0.28^a | 3.30 ± 0.43^b | 5.54 ± 0.40^b | 5.67 ± 0.21^b |

^a $p < 0.05$ relative to the negative control. ^b $p < 0.01$ relative to the negative control. ^c $p < 0.001$ relative to the negative control.

Figure 18. Photographs of DNA comets after electrophoresis of cells in a microgel. (a) Positive control (H_2O_2), (b) Negative control (PBS), and (c–f) $C_{60}(OH)_{24}$ ($C = 10, 50, 75,$ and $100 \mu M$).Table 10. Average Number of Hydrogen Bonds in the Complex of HSA with $C_{60}(OH)_{24}$

| isomer | DS1 | DS2 | DS3 | surface 1 | surface 2 |
|-------------|---------------|---------------|---------------|---------------|---------------|
| uniform | 4.0 ± 1.3 | 3.0 ± 1.6 | 4.0 ± 1.6 | 8.5 ± 2.3 | 2.7 ± 1.3 |
| saturn-like | 4.9 ± 1.3 | 7.4 ± 1.5 | 3.1 ± 2.0 | 7.2 ± 1.9 | 3.6 ± 1.8 |

hemolysis, photobleaching, platelet aggregation, and binding to HSA and DNA. We found that $C_{60}(OH)_{24}$ has low geno- and

cytotoxicity, and it exhibits antiaggregative and antioxidant properties. The study of $C_{60}(OH)_{24}$ binding to HSA

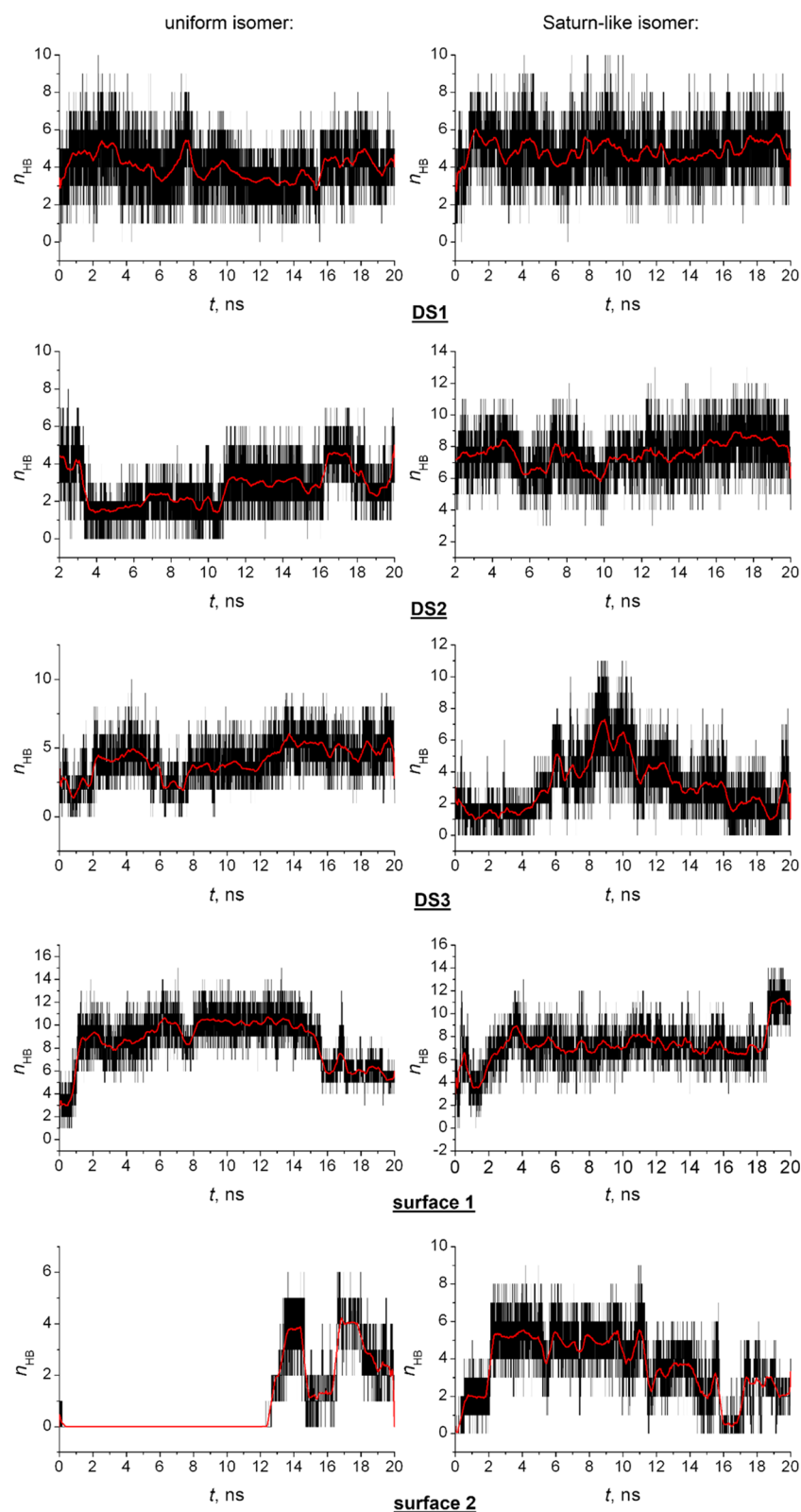


Figure 19. Number of hydrogen bonds between HSA and fullerene $C_{60}(OH)_{24}$ during simulation. The red curve is the result of smoothing.

demonstrated that the interaction of the fullerene with HSA occurs through the subdomains IB (digitonin binding site) and IIIA (ibuprofen binding site); the obtained values of the binding constants indicate that HSA can perform transport functions in the bloodstream. We conclude that $C_{60}(OH)_{24}$ is a promising compound for nanomedicine as a basis for the synthesis of new

biomedical materials, as well as due to its pronounced antioxidant properties. The work showed its high biocompatibility. $C_{60}(OH)_{24}$ also demonstrates increased anticoagulant properties, which make this material promising as a nanomodifier for the development of heart valves and vascular stents.

■ ASSOCIATED CONTENT**SI Supporting Information**

The Supporting Information is available free of charge at <https://pubs.acs.org/doi/10.1021/acs.jpcb.1c03332>.

Intermediate calculation of $C_{60}(\text{OH})_{24}$ –HSA binding data (PDF)

■ AUTHOR INFORMATION**Corresponding Authors**

Vladimir V. Sharoyko – Pavlov First Saint Petersburg State Medical University, Saint Petersburg 197022, Russia; Institute of Chemistry, Saint Petersburg State University, Saint Petersburg 198504, Russia; A. M. Granov Russian Research Centre for Radiology and Surgical Technologies, Saint Petersburg 197758, Russia; Email: sharoyko@gmail.com

Konstantin N. Semenov – Pavlov First Saint Petersburg State Medical University, Saint Petersburg 197022, Russia; Institute of Chemistry, Saint Petersburg State University, Saint Petersburg 198504, Russia; A. M. Granov Russian Research Centre for Radiology and Surgical Technologies, Saint Petersburg 197758, Russia; orcid.org/0000-0003-2239-2044; Email: knsemenov@gmail.com

Authors

Nailia R. Iamalova – Pavlov First Saint Petersburg State Medical University, Saint Petersburg 197022, Russia; Agrophysical Research Institute, Saint Petersburg 195220, Russia

Sergei V. Ageev – Pavlov First Saint Petersburg State Medical University, Saint Petersburg 197022, Russia; Institute of Chemistry, Saint Petersburg State University, Saint Petersburg 198504, Russia

Anatolii A. Meshcheriakov – Pavlov First Saint Petersburg State Medical University, Saint Petersburg 197022, Russia; Institute of Chemistry, Saint Petersburg State University, Saint Petersburg 198504, Russia

Gleb O. Iurev – Pavlov First Saint Petersburg State Medical University, Saint Petersburg 197022, Russia; Almazov National Medical Research Centre, Saint Petersburg 197341, Russia

Andrey V. Petrov – Institute of Chemistry, Saint Petersburg State University, Saint Petersburg 198504, Russia; orcid.org/0000-0002-4650-4891

Dmitry A. Nerukh – Department of Mathematics, Aston University, Birmingham B4 7ET, U.K.; orcid.org/0000-0001-9005-9919

Vladimir S. Farafonov – V. N. Karazin Kharkiv National University, Kharkiv 61022, Ukraine; orcid.org/0000-0003-0785-9582

Lubov V. Vasina – Pavlov First Saint Petersburg State Medical University, Saint Petersburg 197022, Russia

Anastasia V. Penkova – Institute of Chemistry, Saint Petersburg State University, Saint Petersburg 198504, Russia

Complete contact information is available at: <https://pubs.acs.org/doi/10.1021/acs.jpcb.1c03332>

Notes

The authors declare no competing financial interest.

■ ACKNOWLEDGMENTS

This work was supported by a grant from the Russian Science Foundation (20-79-10064). The research was performed using

the equipment of the Resource Center “GeoModel”, Center for Chemical Analysis and Materials Research, Interdisciplinary Resource Center for Nanotechnology, Center for Diagnostics of Functional Materials for Medicine, Pharmacology and Nano-electronics, Magnetic Resonance Research Center, Center for Physical Methods of Surface Investigation, Thermogravimetric and Calorimetric Research Center; computational resources provided by Computer Center of SPbU of the Research Park of Saint Petersburg State University.

■ REFERENCES

- (1) Cataldo, F.; Da Ros, T. Medicinal Chemistry and Pharmacological Potential of Fullerenes and Carbon Nanotubes. In *Carbon Materials: Chemistry and Physics*; Springer Netherlands: Dordrecht, 2008; Vol. 1.
- (2) Piotrovsky, L. B.; Kiselev, O. I. *Fullerenes in Biology*; Rostok: Saint Petersburg, 2006.
- (3) Semenov, K. N.; Charykov, N. A.; Postnov, V. N.; Sharoyko, V. V.; Vorotyntsev, I. V.; Galagudza, M. M.; Murin, I. V. Fullerenols: Physicochemical Properties and Applications. *Prog. Solid State Chem.* **2016**, *44*, 59–74.
- (4) Sforzini, S.; Oliveri, C.; Barranger, A.; Jha, A. N.; Banni, M.; Moore, M. N.; Viarengo, A. Effects of Fullerene C_{60} in Blue Mussels: Role of MTOR in Autophagy Related Cellular/Tissue Alterations. *Chemosphere* **2020**, *246*, No. 125707.
- (5) Lichota, A.; Piwoński, I.; Michlewska, S.; Krokosz, A. A Multiparametric Study of Internalization of Fullereneol $C_{60}(\text{OH})_{36}$ Nanoparticles into Peripheral Blood Mononuclear Cells: Cytotoxicity in Oxidative Stress Induced by Ionizing Radiation. *Int. J. Mol. Sci.* **2020**, *21*, No. 2281.
- (6) Krokosz, A.; Grebowski, J.; Rodacka, A.; Pasternak, B.; Puchala, M. The Effect of Fullereneol $C_{60}(\text{OH})_{30}$ on the Alcohol Dehydrogenase Activity Irradiated with X-Rays. *Radiat. Phys. Chem.* **2014**, *97*, 102–106.
- (7) Erokin, M. Y.; Melenevskaya, E. Y.; Nasonova, K. V.; Bryazhnikova, T. S.; Erokin, E. M.; Danilenko, D. M.; Kiselev, O. I. Synthesis and Biological Activity of Fullereneols with Various Contents of Hydroxyl Groups. *Pharm. Chem. J.* **2013**, *47*, 87–91.
- (8) Yin, J.-J.; Lao, F.; Fu, P. P.; Wamer, W. G.; Zhao, Y.; Wang, P. C.; Qiu, Y.; Sun, B.; Xing, G.; Dong, J.; et al. The Scavenging of Reactive Oxygen Species and the Potential for Cell Protection by Functionalized Fullerene Materials. *Biomaterials* **2009**, *30*, 611–621.
- (9) Mirkov, S. M.; Djordjevic, A. N.; Andric, N. L.; Andric, S. A.; Kostic, T. S.; Bogdanovic, G. M.; Vojinovic-Miloradov, M. B.; Kovacevic, R. Z. Nitric Oxide-Scavenging Activity of Polyhydroxylated Fullereneol, $C_{60}(\text{OH})_{24}$. *Nitric Oxide* **2004**, *11*, 201–207.
- (10) Saitoh, Y.; Miyanishi, A.; Mizuno, H.; Kato, S.; Aoshima, H.; Kokubo, K.; Miwa, N. Super-Highly Hydroxylated Fullerene Derivative Protects Human Keratinocytes from UV-Induced Cell Injuries Together with the Decreases in Intracellular ROS Generation and DNA Damages. *J. Photochem. Photobiol., B* **2011**, *102*, 69–76.
- (11) Jiao, F.; Liu, Y.; Qu, Y.; Li, W.; Zhou, G.; Ge, C.; Li, Y.; Sun, B.; Chen, C. Studies on Anti-Tumor and Antimetastatic Activities of Fullerene in a Mouse Breast Cancer Model. *Carbon* **2010**, *48*, 2231–2243.
- (12) Ma, H.; Zhao, J.; Meng, H.; Hu, D.; Zhou, Y.; Zhang, X.; Wang, C.; Li, J.; Yuan, J.; Wei, Y. Carnosine-Modified Fullerene as a Highly Enhanced ROS Scavenger for Mitigating Acute Oxidative Stress. *ACS Appl. Mater. Interfaces* **2020**, *12*, 16104–16113.
- (13) Đurašević, S.; Nikolić, G.; Todorović, A.; Drakulić, D.; Pejić, S.; Martinović, V.; Mitić-Čulafić, D.; Milić, D.; Kop, T. J.; Jasnjić, N.; et al. Effects of Fullerene C_{60} Supplementation on Gut Microbiota and Glucose and Lipid Homeostasis in Rats. *Food Chem. Toxicol.* **2020**, *140*, No. 111302.
- (14) Thong, N. M.; Vo, Q. V.; Le Huyen, T.; Van Bay, M.; Dung, N. N.; Thu Thao, P. T.; Nam, P. C. Functionalization and Antioxidant Activity of Polyaniline-Fullerene Hybrid Nanomaterials: A Theoretical Investigation. *RSC Adv.* **2020**, *10*, 14595–14605.
- (15) Gudkov, S. V.; Guryev, E. L.; Gapeyev, A. B.; Sharapov, M. G.; Bunkin, N. F.; Shkirin, A. V.; Zabelina, T. S.; Glinushkin, A. P.;

Sevost'yanov, M. A.; Belosludtsev, K. N.; et al. Unmodified Hydrated C₆₀ Fullerene Molecules Exhibit Antioxidant Properties, Prevent Damage to DNA and Proteins Induced by Reactive Oxygen Species and Protect Mice against Injuries Caused by Radiation-Induced Oxidative Stress. *Nanomedicine* **2019**, *15*, 37–46.

(16) Krokosz, A.; Lichota, A.; Nowak, K. E.; Grebowski, J. Carbon Nanoparticles as Possible Radioprotectors in Biological Systems. *Radiat. Phys. Chem.* **2016**, *128*, 143–150.

(17) Jović, D. S.; Seke, M. N.; Djordjevic, A. N.; Mrdanović, J.; Aleksić, L. D.; Bogdanović, G. M.; Pavić, A. B.; Plavec, J. Fullerene Nanoparticles as a New Delivery System for Doxorubicin. *RSC Adv.* **2016**, *6*, 38563–38578.

(18) Tao, R.; Wang, C.; Lu, Y.; Zhang, C.; Zhou, H.; Chen, H.; Li, W. Characterization and Cytotoxicity of Polyphenol Lipid and Vitamin E-TPGS Hybrid Nanoparticles for Betulinic Acid and Low-Substituted Hydroxyl Fullerene in MHCC97H and L02 Cells. *Int. J. Nanomed.* **2020**, *15*, 2733–2749.

(19) Çavaş, T.; Çinkiliç, N.; Vatan, O.; Yılmaz, D. Effects of Fullerene Nanoparticles on Acetamiprid Induced Cytotoxicity and Genotoxicity in Cultured Human Lung Fibroblasts. *Pestic. Biochem. Physiol.* **2014**, *114*, 1–7.

(20) Mrbanovic, Ž.J.; Šolajic, S. V.; Bogdanović, V. V.; Djordjevic, A. N.; Bogdanović, G. M.; Injac, R. D.; Rakočević, Z. L. J. Effects of Fullerene Nano Particles C₆₀(OH)₂₄ on Micronuclei and Chromosomal Aberrations' Frequency in Peripheral Blood Lymphocytes. *Dig. J. Nanomater. Biostructures* **2012**, *7*, 673–686.

(21) Bogdanović, V.; Slavić, M.; Mrdanović, J.; Šolajić, S.; Djordjević, A. The Activity of Superoxide-Dismutase in Animal Cell Culture CHO-K1 after Treatment with Fullerene and Mytomicin C. *Hem. Ind.* **2009**, *63*, 143–149.

(22) Wang, Z.; Wang, S.; Lu, Z.; Gao, X. Syntheses, Structures and Antioxidant Activities of Fullerenols: Knowledge Learned at the Atomistic Level. *J. Cluster Sci.* **2015**, 375–388.

(23) Torres, V. M.; Srdjenovic, B.; Jacevic, V.; Simic, V. D.; Djordjevic, A.; Simplicio, A. L. Fullerene C₆₀(OH)₂₄ Prevents Doxorubicin-Induced Acute Cardiotoxicity in Rats. *Pharmacol. Rep.* **2010**, *62*, 707–718.

(24) Chaudhuri, P.; Paraskar, A.; Soni, S.; Mashelkar, R. A.; Sengupta, S. Fullerene-cytotoxic Conjugates for Cancer Chemotherapy. *ACS Nano* **2009**, *3*, 2505–2514.

(25) Grebinyk, A.; Prylutska, S.; Grebinyk, S.; Prylutsky, Y.; Ritter, U.; Matyshevska, O.; Dandekar, T.; Frohme, M. Complexation with C₆₀ Fullerene Increases Doxorubicin Efficiency against Leukemic Cells In Vitro. *Nanoscale Res. Lett.* **2019**, *14*, No. 61.

(26) Chueh, S. C.; Lai, M. K.; Chen, S. C.; Chiang, L. Y.; Chen, W. C. Fullerenols in Canine Renal Preservation—A Preliminary Report. *Transplant. Proc.* **1997**, *29*, 1313–1315.

(27) Lai, H. S.; Chen, Y.; Chen, W. J.; Chang, J.; Chiang, L. Y. Free Radical Scavenging Activity of Fullerene on Grafts after Small Bowel Transplantation in Dogs. *Transplant. Proc.* **2000**, *32*, 1272–1274.

(28) Ye, S.; Chen, M.; Jiang, Y.; Chen, M.; Wang, Y.; Hou, Z.; Ren, L.; Zhou, T. Polyhydroxylated Fullerene Attenuates Oxidative Stress-Induced Apoptosis via a Fortifying Nrf2-Regulated Cellular Antioxidant Defence System. *Int. J. Nanomed.* **2014**, 2073.

(29) Kamat, J. P.; Devasagayam, T. P. A.; Mohan, H.; Chiang, L. Y.; Mittal, J. P. Effect of C₆₀(OH)₁₈ on Membranes of Rat Liver Microsomes during Photosensitization. *Fullerene Sci. Technol.* **1998**, *6*, 663–679.

(30) Injac, R.; Perse, M.; Obermajer, N.; Djordjevic-Milic, V.; Prijatelj, M.; Djordjevic, A.; Cerar, A.; Strukelj, B. Potential Hepatoprotective Effects of Fullerene C₆₀(OH)₂₄ in Doxorubicin-Induced Hepatotoxicity in Rats with Mammary Carcinomas. *Biomaterials* **2008**, *29*, 3451–3460.

(31) Xu, J.-Y.; Su, Y.-Y.; Cheng, J.-S.; Li, S.-X.; Liu, R.; Li, W.-X.; Xu, G.-T.; Li, Q.-N. Protective Effects of Fullerene on Carbon Tetrachloride-Induced Acute Hepatotoxicity and Nephrotoxicity in Rats. *Carbon* **2010**, *48*, 1388–1396.

(32) Panova, G. G.; Semenov, K. N.; Shilova, O. A.; Khomyakov, Y. V.; Anikina, L. M.; Charikov, N. A.; Artemjeva, A. M.; Kanash, E. V.;

Khamova, T. B.; Udalova, O. R. Water-Soluble Derivatives of Fullerenes and Silicon-Containing Sol-Nanocomposites as the Promising Nanomaterials for Crop Production. *Agrophysica* **2015**, *4*, 37–48.

(33) Bityutskii, N. P.; Yakkonen, K. L.; Lukina, K. A.; Semenov, K. N. Fullerene Increases Effectiveness of Foliar Iron Fertilization in Iron-Deficient Cucumber. *PLoS One* **2020**, *15*, No. e0232765.

(34) Semenov, K. N.; Andrusenko, E. V.; Charykov, N. A.; Litasova, E. V.; Panova, G. G.; Penkova, A. V.; Murin, I. V.; Piotrovskiy, L. B. Carboxylated Fullerenes: Physico-Chemical Properties and Potential Applications. *Prog. Solid State Chem.* **2017**, 47–48, 19–36.

(35) Pochkaeva, E. I.; Podolskiy, N. E.; Zakusilo, D. N.; Petrov, A. V.; Charykov, N. A.; Vlasov, T. D.; Penkova, A. V.; Vasina, L. V.; Murin, I. V.; Sharoyko, V. V.; et al. Fullerene Derivatives with Amino Acids, Peptides and Proteins: From Synthesis to Biomedical Application. *Prog. Solid State Chem.* **2020**, No. 100255.

(36) Sharoyko, V. V.; Ageev, S. V.; Podolskiy, N. E.; Petrov, A. V.; Litasova, E. V.; Vlasov, T. D.; Vasina, L. V.; Murin, I. V.; Piotrovskiy, L. B.; Semenov, K. N. Biologically Active Water-Soluble Fullerene Adducts: Das Glasperlenspiel (by H. Hesse)? *J. Mol. Liq.* **2021**, *323*, No. 114990.

(37) Sharoyko, V. V.; Ageev, S. V.; Meshcheriakov, A. A.; Akentiev, A. V.; Noskov, B. A.; Rakipov, I. T.; Charykov, N. A.; Kulenova, N. A.; Shaimardanova, B. K.; Podolskiy, N. E.; et al. Physicochemical Study of Water-Soluble C₆₀(OH)₂₄ Fullerene. *J. Mol. Liq.* **2020**, *311*, No. 113360.

(38) Markin, A. V.; Samosudova, Y. S.; Ogurtsov, T. G.; Smirnova, N. N.; Ageev, S. V.; Podolskiy, N. E.; Petrov, A. V.; Murin, I. V.; Semenov, K. N. Heat Capacity and Standard Thermodynamic Functions of the Fullerene C₆₀(OH)₂₄. *J. Chem. Thermodyn.* **2020**, *149*, No. 106192.

(39) Djordjević, A.; Vojinović-Miloradov, M.; Petranović, N.; Devečerski, A.; Lazar, D.; Ribar, B. Catalytic Preparation and Characterization of C₆₀Br₂₄. *Fullerene Sci. Technol.* **1998**, *6*, 689–694.

(40) Podolskiy, N. E.; Marcos, M. A.; Cabaleiro, D.; Semenov, K. N.; Lugo, L.; Petrov, A. V.; Charykov, N. A.; Sharoyko, V. V.; Vlasov, T. D.; Murin, I. V. Physico-Chemical Properties of C₆₀(OH)_{22–24} Water Solutions: Density, Viscosity, Refraction Index, Isobaric Heat Capacity and Antioxidant Activity. *J. Mol. Liq.* **2019**, *278*, 342–355.

(41) Semenov, K. N.; Charykov, N. A.; Keskinov, V. N. Fullerene Synthesis and Identification. Properties of the Fullerene Water Solutions. *J. Chem. Eng. Data* **2011**, *56*, 230–239.

(42) Vlakh, E. G.; Grachova, E. V.; Zhukovsky, D. D.; Hubina, A. V.; Mikhailova, A. S.; Shakirova, J. R.; Sharoyko, V. V.; Tunik, S. P.; Tenukova, T. B. Self-Assemble Nanoparticles Based on Polypeptides Containing C-Terminal Luminescent Pt-Cysteine Complex. *Sci. Rep.* **2017**, *7*, No. 41991.

(43) Galebskaya, L. V.; Solovtsova, I. L.; Mikhailova, I. A. *Device for the Study of Photoinduced Cytolysis*, RU114157U1, 2012.

(44) Galebskaya, L. V.; Solovtsova, I. L.; Miroshnikova, E. B.; Mikhailova, I. A.; Sushkin, M. E.; Razumny, A. V.; Babina, A. V.; Fomina, V. A. The Importance of a Photosensitizer Bleaching Registration for the Evaluation of Mechanism of Preparation Action on the Photo-Induced Hemolysis. *Biomed. Photonics* **2017**, *6*, 33–38.

(45) Mandal, S.; Hazra, B.; Sarkar, R.; Biswas, S.; Mandal, N. Assessment of the Antioxidant and Reactive Oxygen Species Scavenging Activity of Methanolic Extract of Caesalpinia Crista Leaf. *Evidence-Based Complementary Altern. Med.* **2011**, *2011*, No. 173768.

(46) Oyaizu, M. Studies on Products of Browning Reaction. Antioxidative Activities of Products of Browning Reaction Prepared from Glucosamine. *Jpn. J. Nutr. Diet.* **1986**, *44*, 307–315.

(47) Bursal, E.; Köksal, E. Evaluation of Reducing Power and Radical Scavenging Activities of Water and Ethanol Extracts from Sumac (*Rhus coriaria* L.). *Food Res. Int.* **2011**, *44*, 2217–2221.

(48) Hadjur, C.; Lange, N.; Rebstain, J.; Monnier, P.; van den Bergh, H.; Wagnières, G. Spectroscopic Studies of Photobleaching and Photoproduct Formation of Meta(Tetrahydroxyphenyl)Chlorin (m-THPC) Used in Photodynamic Therapy. The Production of Singlet Oxygen by m-THPC. *J. Photochem. Photobiol., B* **1998**, *45*, 170–178.

(49) Keeffe, J. *ThermoFluor Assay Protocol*; 2013.

- (50) Vivoli, M.; Novak, H. R.; Littlechild, J. A.; Harmer, N. J. Determination of Protein-Ligand Interactions Using Differential Scanning Fluorimetry. *J. Vis. Exp.* **2014**, No. 91, No. 51809.
- (51) Gaponenko, I. N.; Ageev, S. V.; Iurev, G. O.; Shemchuk, O. S.; Meshcheriakov, A. A.; Petrov, A. V.; Solovtsova, I. L.; Vasina, L. V.; Tennikova, T. B.; Murin, I. V.; et al. Biological Evaluation and Molecular Dynamics Simulation of Water-Soluble Fullerene Derivative $C_{60}[C(COOH)_2]_3$. *Toxicol. Vitro.* **2020**, 62, No. 104683.
- (52) Olive, P. L.; Banáth, J. P.; Durand, R. E.; Banath, J. P. Heterogeneity in Radiation-Induced DNA Damage and Repair in Tumor and Normal Cells Measured Using the "Comet" Assay. *Radiat. Res.* **1990**, 122, 86–94.
- (53) Abraham, M. J.; Murtola, T.; Schulz, R.; Páll, S.; Smith, J. C.; Hess, B.; Lindah, E. GROMACS: High Performance Molecular Simulations through Multi-Level Parallelism from Laptops to Supercomputers. *SoftwareX* **2015**, 1–2, 19–25.
- (54) Humphrey, W.; Dalke, A.; Schulten, K. VMD: Visual Molecular Dynamics. *J. Mol. Graph.* **1996**, 14, 33–38.
- (55) Robertson, M. J.; Tirado-Rives, J.; Jorgensen, W. L. Improved Peptide and Protein Torsional Energetics with the OPLS-AA Force Field. *J. Chem. Theory Comput.* **2015**, 11, 3499–3509.
- (56) Vanqualef, E.; Simon, S.; Marquant, G.; Garcia, E.; Klimerak, G.; Delepine, J. C.; Cieplak, P.; Dupradeau, F.-Y. R.E.D. Server: A Web Service for Deriving RESP and ESP Charges and Building Force Field Libraries for New Molecules and Molecular Fragments. *Nucleic Acids Res.* **2011**, 39, W511–W517.
- (57) Girifalco, L. A. Molecular Properties of C_{60} in the Gas and Solid Phases. *J. Phys. Chem. A* **1992**, 96, 858–861.
- (58) Huang, Z. R.; Hua, S. C.; Yang, Y. L.; Fang, J. Y. Development and Evaluation of Lipid Nanoparticles for Camptothecin Delivery: A Comparison of Solid Lipid Nanoparticles, Nanostructured Lipid Carriers, and Lipid Emulsion. *Acta Pharmacol. Sin.* **2008**, 29, 1094–1102.
- (59) Senge, M. O.; Brandt, J. C. Temoporfin (Foscan, 5,10,15,20-Tetra(m-Hydroxyphenyl)Chlorin) - A Second-Generation Photosensitizer. *Photochem. Photobiol.* **2011**, 1240–1296.
- (60) Golomidov, I.; Bolshakova, O.; Komissarov, A.; Sharoyko, V.; Slepneva, E.; Slobodina, A.; Latypova, E.; Zherybateva, O.; Tennikova, T.; Sarantseva, S. The Neuroprotective Effect of Fullerenols on a Model of Parkinson's Disease in *Drosophila Melanogaster*. *Biochem. Biophys. Res. Commun.* **2020**, 523, 446–451.
- (61) Grebowski, J.; Konopko, A.; Krokosz, A.; DiLabio, G. A.; Litwinienko, G. Antioxidant Activity of Highly Hydroxylated Fullerene C_{60} and Its Interactions with the Analogue of α -Tocopherol. *Free Radic. Biol. Med.* **2020**, 160, 734–744.
- (62) Srdjenovic, B.; Milic-Torres, V.; Grujic, N.; Stankov, K.; Djordjevic, A.; Vasovic, V. Antioxidant Properties of Fullereneol $C_{60}(OH)_{24}$ in Rat Kidneys, Testes, and Lungs Treated with Doxorubicin. *Toxicol. Mech. Methods* **2010**, 20, 298–305.
- (63) Kovel, E. S.; Sachkova, A. S.; Vnukova, N. G.; Churilov, G. N.; Knyazeva, E. M.; Kudryasheva, N. S. Antioxidant Activity and Toxicity of Fullerenols via Bioluminescence Signaling: Role of Oxygen Substituents. *Int. J. Mol. Sci.* **2019**, 20, No. 2324.
- (64) He, X. M.; Carter, D. C. Atomic Structure and Chemistry of Human Serum Albumin. *Nature* **1992**, 358, 209–215.
- (65) Tang, J.; Luan, F.; Chen, X. Binding Analysis of Glycyrrhetic Acid to Human Serum Albumin: Fluorescence Spectroscopy, FTIR, and Molecular Modeling. *Bioorg. Med. Chem.* **2006**, 14, 3210–3217.
- (66) Ungurenasu, C.; Pinteala; Dascalu. Binding Fullereneol $C_{60}(OH)_{24}$ to DsDNA. *Int. J. Nanomed.* **2009**, 4, 193.
- (67) Mrđanović, J.; Solajić, S.; Bogdanović, V.; Stankov, K.; Bogdanović, G.; Djordjevic, A. Effects of Fullereneol $C_{60}(OH)_{24}$ on the Frequency of Micronuclei and Chromosome Aberrations in CHO-K1 Cells. *Mutat. Res. Toxicol. Environ. Mutagen.* **2009**, 680, 25–30.
- (68) Serebryakov, E. B.; Zakusilo, D. N.; Semenov, K. N.; Charykov, N. A.; Akentiev, A. V.; Noskov, B. A.; Petrov, A. V.; Podolsky, N. E.; Mazur, A. S.; Dul'neva, L. V.; et al. Physico-Chemical Properties of C_{70} -L-Threonine Bisadduct ($C_{70}(C_4H_9NO_2)_2$) Aqueous Solutions. *J. Mol. Liq.* **2019**, 279, 687–699.